J. Fac. Sci. Univ. Tokyo
Sect. IA, Math.
36 (1989), 571-613.

New bifurcation diagrams in the problem of permanent progressive waves

Dedicated to Professor Hiroshi Fujita on his 60th birthday

By Mayumi SHŌJI

Abstract. Plane progressive waves on water of finite or infinite depth are treated under the effect of both gravity and surface tension. We are interested in the bifurcation phenomena, particularly in Wilton's waves which are obtained as a consequence of bifurcation of multiplicity two. We obtain bifurcating solutions and their bifurcation diagrams numerically. We include into solutions those waves in which the flow regions have self-intersections. By this, we see qualitative agreement of the numerical results with the mathematical theory.

§ 0. Introduction.

We consider a problem of progressive water waves. Our objective is to study a bifurcation structure, particularly the one near a critical point of multiplicity two, by numerical and analytical methods. We consider a two dimensional irrotational flow of inviscid incompressible fluid with a free surface. What will be considered here is called a progressive wave, by which we mean a fluid motion with free surface whose shape is constant if viewed in a moving frame. We take an x-y coordinate system moving in the same direction as the wave with the same speed c (see Figure 1). We first consider the flow of infinite depth. The case of finite depth will be considered in a later section. The free boundary is represented by a function H as $\{(x, y) \mid y=H(x)\}$. Accordingly the fluid region is $\{(x, y) \mid -\infty<x<\infty,\ -\infty<y<H(x)\}$. We assume a conventional hypothesis that the wave profile is symmetric about y-axis and is periodic in x of the period, say, L. By the periodicity, we have only to consider the fluid in $\{-L/2<x<L/2,\ -\infty<y<H(x)\}$. Then the problem is to find a wave profile function $y=H(x)$ and a complex potential $w\equiv U+iV$, where U is a velocity potential and V is a stream function, such that $U+iV$ is a holomorphic function of $z\equiv x+iy$ and satisfies

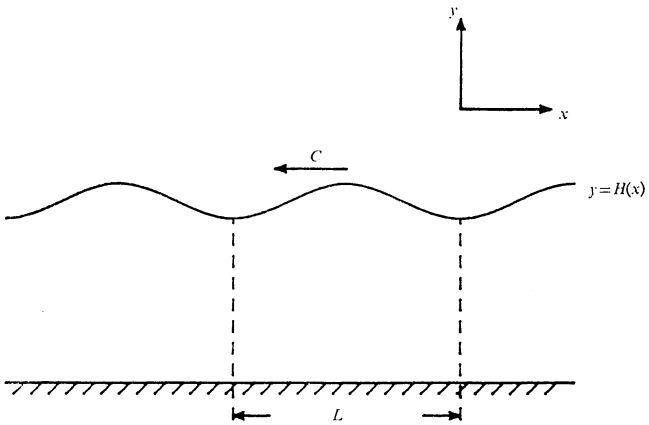

Figure 1. Periodic progressive wave on water of finite or infinite depth.

$$U\left(\pm\frac{L}{2}, y\right)=\pm\frac{cL}{2} \qquad \text{(respectively)},$$

$$V=0 \qquad \text{on} \quad y=H(x),$$

$$U+iV \longrightarrow cz \qquad \text{as} \quad y\to-\infty,$$

$$\frac{1}{2}\left|\frac{dw}{dz}\right|^2+gy-TK=\text{constant} \qquad \text{on} \quad y=H(x).$$

Here g is the gravity acceleration, T is the surface tension coefficient, K is the curvature of the boundary $y=H(x)$ and $i=\sqrt{-1}$. We note that "$w(z)=cz$" and "$H(x)\equiv$constant" solve this problem. We call this a trivial solution. We are interested in non-trivial solutions bifurcating from the trivial one. There are two extreme cases. The waves in the case of $T=0$ are called pure gravity waves. Those in the case of $g=0$ are called pure capillary waves. We call waves for general (g, T) capillary-gravity waves. Crapper [4] presented exact expression for pure capillary waves of infinite depth in terms of elementary functions. The wave profiles calculated by his formula are given in Figure 2. Later, Kinnersley [8] gave an expression for pure capillary waves of finite depth in terms of elliptic functions. Thus, complete solutions are obtained in the case of $g=0$. However, in the case of general capillary-gravity waves, explicit solutions are no more available. On the other hand, abstract mathematical proofs are given to the existence of bifurcating solutions in general cases ([10, 11, 16, 19, 20]). The validity of the

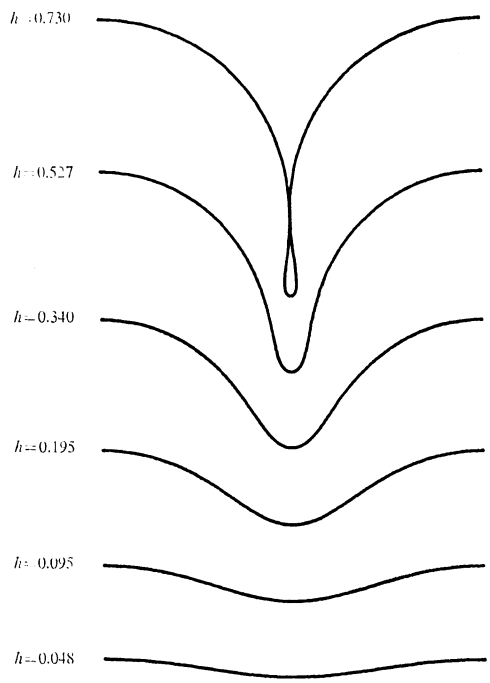

Figure 2. Profiles for different heights for Crapper's exact solution of progressive capillary waves (i.e. $g=0$). Here h indicates the amplitude of wave.

mathematical theory is, however, limited to a small neighborhood of the trivial solution. Chen and Saffman [1, 2] computed solutions numerically and found new capillary-gravity waves although they do not give a mathematical proof of existence. We follow the method in [1, 2], which is called the Stokes expansion method. But we execute numerical computation more systematically and give solutions which are not given in [1, 2]. We also present the bifurcation diagrams and show how they change as the parameters vary.

The present paper is composed of five sections. In § 1 we state how we discretize the problem. §§ 2, 3 contains the explanations for the numerical results. In § 2 we also mention about the case of finite depth. § 4 is devoted to discussions.

§ 1. Formulation.

Under the assumption in § 0, we may restrict ourselves to $\Omega_H \equiv$

$\{(x, y) \mid |x|<L/2,\ -\infty<y<H(x)\}$. The problem to be considered is formulated as follows:

Problem. Find functions $H=H(x)$ $(-L/2<x<L/2)$, $U(x, y)$ and $V(x, y)$ $(-L/2<x<L/2,\ -\infty<y<H(x))$ satisfying the following (1-5):

(1) $w=w(z)=U+iV$ is a complex analytic function of $z=x+iy$ in Ω_H,

(2) $H(x)$ and $\dfrac{dw}{dz}$ are periodic functions of x with a period L,

(3) $V=0$ on $y=H(x)$, $U+iV\longrightarrow cz$ as $y\to-\infty$,

(4) $U\left(\pm\dfrac{L}{2}, y\right)=\pm\dfrac{L}{2}c$ (respectively),

(5) $\dfrac{1}{2}\left|\dfrac{dw}{dz}\right|^2+gH-T\left(\dfrac{H_x}{(1+H_x^2)^{1/2}}\right)_x=$constant on $y=H(x)$,

where c, g and T are prescribed positive constants. Subscripts mean differentiations. c is a propagation speed. g is the gravity acceleration and T is the surface tension coefficient. Here we remark that the constant of the right hand side of (5) depends on c and the choice of the origin.

There is a mathematical difficulty for solving (1-5): the boundary portion $\{y=H(x)\}$ is unknown. In order to overcome this difficulty, we follow the happy idea due to Stokes that we regard z as a function of w. Thus we seek a solution of the following form:

$$(6)\qquad z=x+iy=\frac{w}{c}+\sum_{j=1}^{\infty}\frac{iL(A_j+iB_j)}{2\pi j}\exp\left(-\frac{2j\pi iw}{cL}\right)+\frac{iL(A_0+iB_0)}{2\pi},$$

where $A_j, B_j\in\boldsymbol{R}$ are unknowns to be sought (see [1]). We call expansions of this form the Stokes expansion. We consider only symmetric waves, so we put $B_j=0$ for all $j\geq1$ in (6). The constant terms, A_0 and B_0, are determined by positioning of the origin. Therefore they do not affect wave profiles. The function $z=z(w)$ is defined in $\{|U|\leq cL/2,\ -\infty<V\leq0\}$. Therefore the free boundary problem is transformed to a problem of fixed domain. From (3), the free surface $\{(x, y)\mid y=H(x)\}$ is given by putting $V=0$ in (6). This gives us

$$x=\frac{U}{c}+\frac{L}{2\pi}\sum_{1}^{\infty}\frac{A_j}{j}\sin\left(\frac{2j\pi U}{cL}\right)+\frac{LB_0}{2\pi},$$

$$y=\frac{L}{2\pi}\sum_{1}^{\infty}\frac{A_j}{j}\cos\left(\frac{2j\pi U}{cL}\right)+\frac{LA_0}{2\pi}.$$

Our task is, therefore, to determine $A_j's$ $(j=1, 2, \cdots)$. We determine them by the condition (5). We represent the condition (5) in terms of x and y above. As for the first term $|dw/dz|^2$, we have the following expression: on the free surface, the stream function V is constant, hence we have $dw\equiv dU$ there. Consequently $dz/dw=dz/dU=dx/dU+idy/dU$, and $|dz/dw|^2=(dx/dU)^2+(dy/dU)^2$. Similarly we express the curvature $-(H_x/(1+H_x^2)^{1/2})_x$ by means of dU. Thus we have the following equivalent expression for (5):

$$\frac{1}{2}\frac{1}{\dot{x}^2+\dot{y}^2}+gy-T\frac{\dot{x}\ddot{y}-\ddot{x}\dot{y}}{(\dot{x}^2+\dot{y}^2)^{3/2}}=\text{constant}, \tag{5'}$$

where $\cdot$ represents derivatives with respect to U.

We now introduce non-dimensional variables. We put $\xi=2\pi U/cL$ and $X(\xi)=x(U)2\pi/L$, $Y(\xi)=y(U)2\pi/L$. Then we have

$$X(\xi)=\xi+\sum_{1}^{\infty}\frac{A_j}{j}\sin(j\xi)+B_0, \qquad Y(\xi)=\sum_{1}^{\infty}\frac{A_j}{j}\cos(j\xi)+A_0. \tag{7}$$

By the relations $\dot{x}=X'/c$, $\dot{y}=Y'/c$, $\ddot{x}=2\pi X''/c^2L$ and $\ddot{y}=2\pi Y''/c^2L$, (5′) is now written as

$$\frac{\mu}{2}\frac{1}{X'^2+Y'^2}+Y-\kappa\frac{X'Y''-X''Y'}{(X'^2+Y'^2)^{3/2}}=\text{constant}, \tag{8}$$

where $'$ represents derivatives with respect to ξ and we have put

$$\mu=\frac{2\pi c^2}{gL}, \qquad \kappa=\frac{4\pi^2T}{gL^2}. \tag{9}$$

Chen and Saffman used the above equation (8). We, however, prefer the following differential form (8′) of (8) since it is convenient in order to apply bifurcation theory given by Crandall and Rabinowitz and others:

$$\frac{\mu}{2}\frac{d}{d\xi}\frac{1}{X'^2+Y'^2}+Y'-\kappa\frac{d}{d\xi}\frac{X'Y''-X''Y'}{(X'^2+Y'^2)^{3/2}}=0. \tag{8'}$$

The task is to solve (8′) with (7, 9), i.e., to find $(A_1, A_2, \cdots)$ satisfying (8′) for given κ, μ. Since only the derivatives of X and Y appear in (8′), we use instead of (7) the following

$$X'(\xi)=1+\sum_1^\infty A_j\cos(j\xi),\qquad Y'(\xi)=-\sum_1^\infty A_j\sin(j\xi). \tag{10}$$

Note that the constant terms, A_0 and B_0, disappear and we have a formulation which is closed in $(A_1, A_2, \cdots)$. To state in a more mathematical fashion, we rewrite this problem as a problem to seek zero points of a mapping F which we will define below. For a given $(A_1, A_2, \cdots)$, we define $\Psi(\xi)$ by

$$\Psi(\xi)=\frac{\mu}{2}\frac{1}{X'^2+Y'^2}+Y-\kappa\frac{X'Y''-X''Y'}{(X'^2+Y'^2)^{3/2}}. \tag{11}$$

We then define a mapping by $F(\kappa, \mu; A_1, A_2, \cdots)=(A_1^*, A_2^*, \cdots, B_1^*, B_2^*, \cdots)$. Here A_j^* and B_j^* are defined by

$$A_j^*=\frac{1}{\pi}\left(\frac{d}{d\xi}\Psi(\xi),\ \sin(j\xi)\right)=\frac{1}{\pi}(\Psi(\xi),\ -j\cos(j\xi)), \tag{12}$$

and

$$B_j^*=-\frac{1}{\pi}\left(\frac{d}{d\xi}\Psi(\xi),\ \cos(j\xi)\right)=-\frac{1}{\pi}(\Psi(\xi),\ j\sin(j\xi)). \tag{13}$$

Each B_j^* for $j\geq 1$ in (13) vanishes since $X(\xi)$ is odd in ξ, $Y(\xi)$ is even and $\Psi(\xi)$ is even. Consequently, so as to seek zero points of F, our task is only to solve

$$F(\kappa, \mu;\ A_1, A_2, \cdots)\equiv(A_1^*, A_2^*, \cdots)=0 \tag{14}$$

for given κ and μ.

For a bifurcation theoretic analysis, the following proposition is a basis.

PROPOSITION. i) $F(\kappa, \mu;\ 0, 0, \cdots)\equiv 0$, *i.e.* $(A_1, A_2, \cdots)=(0, 0, \cdots)$ *is a solution for all* κ *and* μ, ii) *the Fréchet derivative of* F *at* $(A_1, A_2, \cdots)=(0, 0, \cdots)$ *fails to be an isomorphism if and only if* $\mu=1/m+m\kappa$ *for some positive integer* m.

PROOF: i) is easy to see. ii) is proved by the following formula for the Fréchet derivative DF:

$$DF(\kappa, \mu;\ 0, 0, \cdots)(A_1, A_2, \cdots)=\sum_{j=1}^\infty\{\mu j-1-\kappa j^2\}A_j\sin(j\xi). \qquad \blacksquare$$

Now we introduce the following symbol and definitions:

$$S_m=\left\{(\kappa,\mu)\,\middle|\,\mu=\frac{1}{m}+m\kappa\right\}\qquad\text{for}\quad m\in N.$$

DEFINITION. If $(\kappa,\mu)\in S_n$ and $(\kappa,\mu)\notin S_m$ $(\forall m\neq n)$, then we call (κ,μ) *a simple bifurcation point of mode* n.

DEFINITION. Let m, n be integers such that $0<m<n$. If $(\kappa,\mu)\in S_m\cap S_n$ and $(\kappa,\mu)\notin S_l$ $(\forall l\neq m,n)$, then we call (κ,μ) *a double bifurcation point of mode* (m,n).

The set S_m is a straight line and the intersection of S_m and S_n $(m\neq n)$ is the double bifurcation point of mode (m,n), which is denoted by $S_{m,n}$. Let m and n be fixed integers such that $0<m<n$ and let (κ_0,μ_0) be the double bifurcation point of mode (m,n). Then we have

$$\kappa_0=\frac{1}{mn},\qquad \mu_0=\frac{m+n}{mn}. \tag{15}$$

We will see there are secondary bifurcations in a neighborhood of $S_{m,n}$.

We now describe our numerical algorithm to obtain bifurcating solutions from S_m and $S_{m,n}$, and to obtain secondary bifurcating solutions.

I) The case of simple bifurcation point

Let $m\in N$ be given and κ_0 be fixed. Let (κ_0,μ_0) be a simple bifurcation point of mode m.

By truncation we define an approximate equation of (14) as follows:

$$F^{(N)}(\kappa,\mu;\ A_1,A_2,\cdots,A_N)=(A_1^*,A_2^*,\cdots,A_N^*),$$

where A_j^* is defined by (11, 12) with $(A_1,A_2,\cdots)$ replaced by $(A_1,A_2,\cdots,A_N,0,\cdots)$. Then the discrete version of our problem is of the following form.

$$\begin{aligned}&(H_1(\lambda,A_1,\cdots,A_N;\ \kappa_0),\ H_2(\cdots),\cdots,H_N(\cdots))\\&\quad\equiv F^{(N)}(\kappa_0,\mu_0+\lambda;\ A_1,\cdots,A_N)=0.\end{aligned} \tag{16}$$

Here we have N equations for $N+1$ unknowns $(\lambda,A_1,\cdots,A_N)$. One more equation should be supplied to control bifurcation parameter λ. There are several possibilities. In some case, we use

$$H_{N+1}(\lambda,A_1,\cdots,A_N;\ \kappa_0)\equiv\lambda-\tilde{\lambda}=0, \tag{17}$$

where $\tilde{\lambda}$ is a suitably chosen constant. In other situation (17) becomes

unsuitable and we switch (17) to

$$H_{N+1}(\lambda, A_1, \cdots, A_N;\ \kappa_0)\equiv A_m-\tilde{A}_m=0, \tag{18}$$

where $\tilde{A}_m$ is a suitably chosen constant. Whether we use (17) or (18) depends on the direction of solution arc. Now $H\equiv(H_1, H_2, \cdots, H_{N+1})^t=0$ gives $N+1$ nonlinear equations for the $N+1$ unknowns, and this system can be solved by the Euler-Newton method:

$$DH^p\cdot\begin{pmatrix}\lambda^{p+1}-\lambda^p\\ A_1^{p+1}-A_1^p\\ \vdots\\ A_N^{p+1}-A_N^p\end{pmatrix}=-H(\lambda^p, A_1^p, \cdots, A_N^p). \tag{19}$$

Here p indicates p-th step of iterations and DH^p is the Jacobian matrix of H at $(\lambda, A_1, \cdots, A_N)=(\lambda^p, A_1^p, \cdots, A_N^p)$. The most time-consuming part in this algorithm is the computation of DH. But the FFT method is effectively used to construct this matrix. In fact, the kth row of DH is composed of cosine coefficients such as

$$\begin{cases}\dfrac{\partial H_j}{\partial\lambda}=-\dfrac{j}{\pi}\left(\dfrac{\partial}{\partial\lambda}\Psi(\xi),\ \cos(j\xi)\right) & \text{for}\quad k=1,\\[2ex] \dfrac{\partial H_j}{\partial A_{k-1}}=-\dfrac{j}{\pi}\left(\dfrac{\partial}{\partial A_{k-1}}\Psi(\xi),\ \cos(j\xi)\right) & \text{for}\quad k\neq 1,\end{cases} \tag{20}$$

where we can write $\partial\Psi/\partial\lambda$ and $\partial\Psi/\partial A_{k-1}$ concretely. Therefore (20) is an explicit representation.

After all, the algorithm to solve bifurcating solutions of mode m is described as follows: Let ε be suitably chosen, positive or negative. We take a first approximation $(\lambda^0, A_1^0, \cdots, A_m^0, \cdots, A_N^0)=(0, 0, \cdots, \overset{m+1}{\check{\varepsilon}}, \cdots, 0)$ and solve the Euler-Newton's scheme (19) where (18) with $\tilde{A}_m=\varepsilon$ is adopted. When $|(\lambda^{p+1}, A_1^{p+1}, \cdots, A_N^{p+1})-(\lambda^p, A_1^p, \cdots, A_N^p)|$ becomes smaller than a prescribed small value, we employ $(\lambda^{p+1}, A_1^{p+1}, \cdots, A_N^{p+1})$ as the solution for the given ε. In the next step, we repeat the same procedure for $\varepsilon+\delta\varepsilon$ where $\delta\varepsilon$ is a small increment, taking the previously obtained bifurcating solution as the first approximation for the present step. We continue this procedure. If the iteration does not converge, we choose a new $\delta\varepsilon$ smaller than the previous one and compute again. If the iteration does not converge for very small $\delta\varepsilon$, we are approaching either

a limit point or a singular point. Some authors call the former a turning point (in the A_m-direction). The latter is one of secondary bifurcation points. In the first case, we can similarly continue the above procedure by switching (18) to (17). In the second case, we can skip the bifurcation point by letting $\delta\varepsilon$ be larger and continue the above procedure again. After obtaining the primary branch, we come back to the (secondary) bifurcation point and compute the secondary bifurcating solutions as is described in Keller [9] (see III) below). In this way, we can get the global bifurcation branch.

II) The case of double bifurcation point

Even in this case, the procedure is essentially the same as before. However, there are intersections at which two or more branches meet. Accordingly we must choose initial approximations appropriately. Below, we state how to decide a suitable initial value. Let (κ_0, μ_0) be a double bifurcation point of mode (m, n).

Bifurcating solutions from $S_{m,n}$ are waves such that A_m and A_n are of comparable order and the remaining A_j $(j \neq m, n)$ are of smaller order. An initial guess is obtained by neglecting terms in $\Psi(\xi)$ of order smaller than $O(|A_m+A_n|^3)$. To put it concretely, let us explain by examples. We put $m=1$ and $n=2$. We then have $(\kappa_0, \mu_0)=(1/2, 3/2)$ by (15). By $H_j=0$ $(j=1, 2)$ of (16), we obtain after some manipulation the following

$$(1-\mu+\kappa)A_1+\left(\mu-\frac{3}{2}\kappa\right)A_1A_2+O(|A_1+A_2|^3)=0, \tag{21}$$

$$\left(\frac{1}{2}-\mu+2\kappa\right)A_2+\left(-\frac{1}{2}\mu-\frac{3}{2}\kappa\right)A_1^2+O(|A_1+A_2|^3)=0. \tag{22}$$

Here, κ is fixed to $\kappa_0(=1/2)$. We now consider the solutions in which $A_1 \neq 0$. We neglect the terms of order ≥ 3 and divide (21) by A_1 to have

$$\left(\frac{3}{2}-\mu\right)+\left(\mu-\frac{3}{4}\right)A_2=0, \qquad \left(\frac{3}{2}-\mu\right)A_2+\left(-\frac{1}{2}\mu-\frac{3}{4}\right)A_1^2=0.$$

These two equations give

$$\mu=\left(\frac{3}{2}-\frac{3}{4}A_2\right)\Big/(1-A_2)=\mu_0+\frac{3}{4}A_2+O(|A_2|^2), \qquad A_1=\pm A_2.$$

Namely we obtain two initial approximations: $(\lambda^0, A_1^0, A_2^0, A_3^0, \cdots, A_N^0)=(0.75\varepsilon, \pm\varepsilon, \varepsilon, 0, \cdots, 0)$.

When $m=1$ and $n=3$, we can obtain the following two equations from $H_j=0$ $(j=1, 2, 3, 4, 6)$ of (16) in the same way as above:

$$\frac{A_1}{A_3}=-0.763\cdots,\ -0.187\cdots,\ 1.202\cdots, \qquad \mu=\frac{4}{3}+\frac{23}{36}A_3^2=\mu_0+O(|A_3|^2).$$

Thus we have three initial approximations: $(\lambda^0, A_1^0, A_2^0, A_3^0, \cdots, A_N^0)=(0, -0.763\varepsilon, 0, \varepsilon, 0, \cdots, 0)$, $(0, -0.187\varepsilon, 0, \varepsilon, 0, \cdots, 0)$ and $(0, 1.202\varepsilon, 0, \varepsilon, 0, \cdots, 0)$.

III) The case of secondary bifurcation

If the parameters are perturbed from the double bifurcation point, there appear secondary bifurcations. For such values of parameters, we need to calculate eigenvalues of DH in every step of obtaining one bifurcating solution in the procedure of I). When some of the eigenvalues change their signs, there exist some singular points which are either of secondary bifurcation point or of turning point. After calculating all primary bifurcating solutions of mode m, we return to the neighborhood of each singular point and find its accurate location by bisection method. In order to determine whether it is a bifurcation point or a turning point, we employ Keller's method. By the method, we can find a secondary bifurcation point and a direction of secondary branch. In order to switch branches at bifurcation points, we can use Keller's method.

§ 2. Results for the bifurcation of mode (1, 2).

In this and the next sections we show our results of numerical computation. All the solutions presented in this section are found in a neighborhood of the double bifurcation point of mode (1, 2).

Let (κ_0, μ_0) be the double bifurcation point of mode (1, 2). Since $m=1$ and $n=2$, it holds by (15) that $\kappa_0=0.5$ and $\mu_0=1.5$. If we change κ slightly from $\kappa_0=0.5$, there appear secondary bifurcations as will be shown below.

First, we explain Figures 3-6, which are the results for $\kappa=0.7(>\kappa_0)$. $(\kappa, \mu)=(0.7, 1.7)$ is the simple bifurcation point of mode 1 and $(\kappa, \mu)=(0.7, 1.9)$ is that of mode 2. Figures 3-5 show wave profiles which are drawn in one wavelength, namely in a range of $0\leq\xi\leq 2\pi$ (i.e., $0\leq x\leq L$). Figure 3 shows solutions along the branch of mode 1. The wave profile of mode 1 changes from wave of small amplitude like $\cos(\theta)$ to the highest wave enclosing a bubble like Crapper's wave. Both of the wave amplitude and the bubble are smaller than those of Crapper's wave.

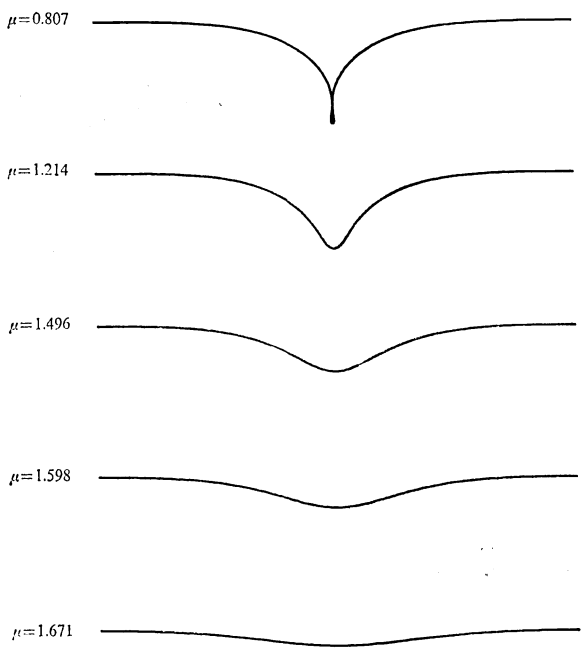

Figure 3. Profiles of mode 1 waves for $\kappa=0.7$ of infinite depth.

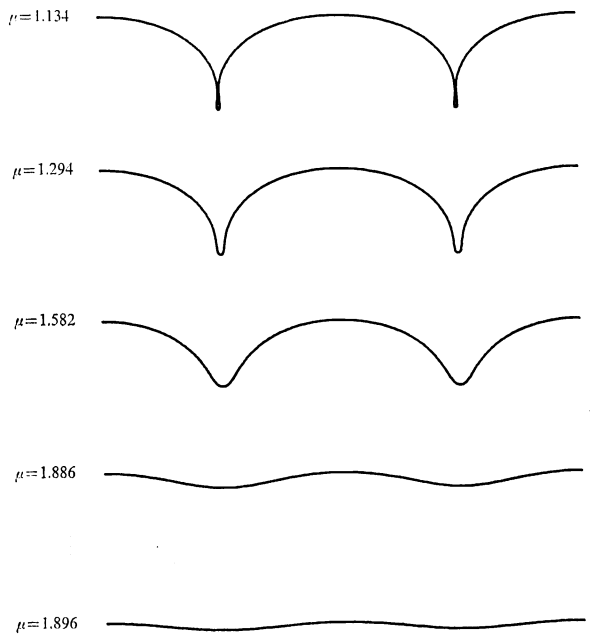

Figure 4. Profiles of mode 2 waves for $\kappa=0.7$ of infinite depth.

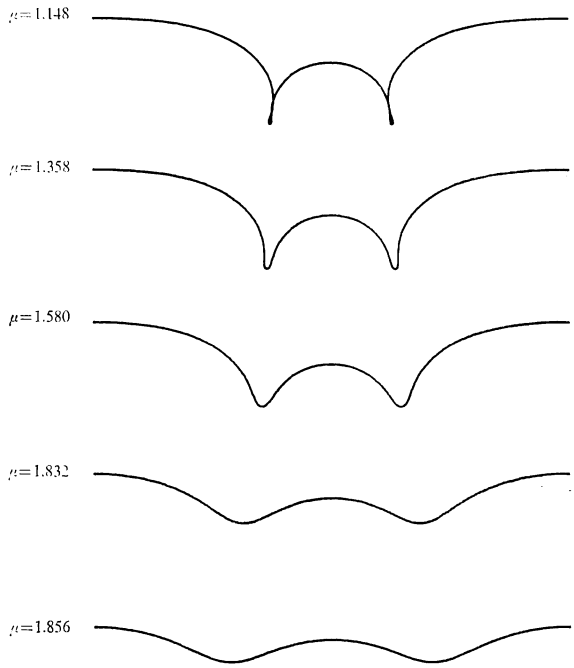

Figure 5. Profiles of mode (1, 2) combination waves for $\kappa=0.7$ of infinite depth. A secondary bifurcation point is $\mu=1.859$.

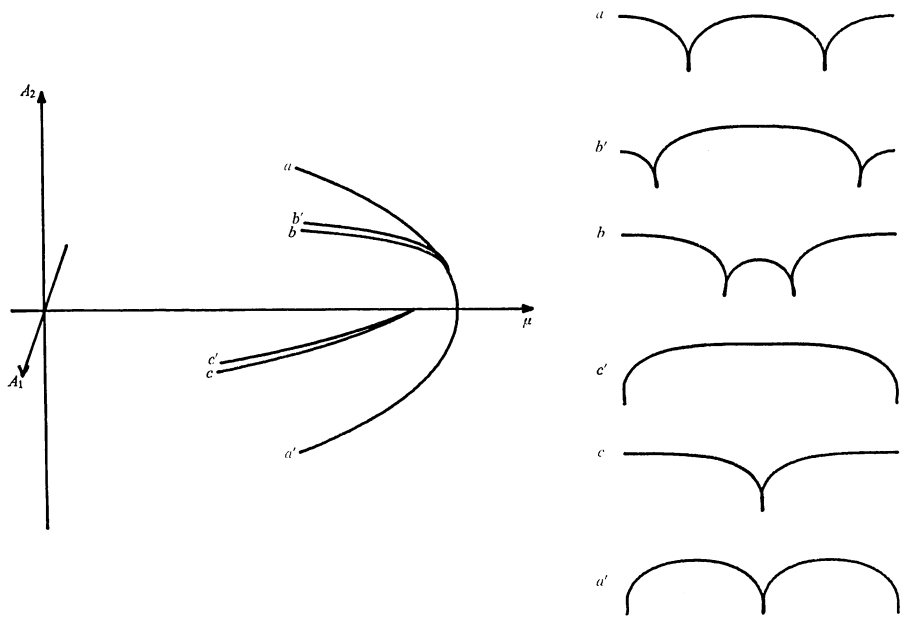

Figure 6. Bifurcation branches for $\kappa=0.7$ of infinite depth.

Figure 4 shows solutions along the branch of mode 2. The wave profile of mode 2 changes from wave of small amplitude like $\cos(2\theta)$ to the highest wave where the surface encloses two bubbles. Figure 5 shows solutions along secondary branch which bifurcates subcritically from the branch of mode 2. The secondary bifurcation point is calculated as $(\kappa, \mu)=(0.7,\ 1.859\cdots)$. The surface of the highest wave also encloses two bubbles. In Figure 6 the bifurcation diagram for $\kappa=0.7$ is drawn, where all branches bifurcate subcritically and the bifurcations are pitchforks. The branch of mode 2 is on μ-A_2 plane and is symmetric about μ-A_1 plane. A bifurcating solution on the lower side corresponds to a phase shift of $\pi/2$ of the solution at the symmetric point on the upper side (see wave profiles a and a' in Figure 6). Similarly, the branches of mode 1 and the secondary branches are symmetric about μ-A_2 plane. Bifurcating solutions located symmetrically are obtained by phase shift of π (see figures b, c and b', c' in Figure 6). Here phase shift of $\pi/2$ (or π) is equivalent to moving the origin horizontally by $L/4$ (or $L/2$). Chen and Saffman [1, 2] gave wave profiles in Figure 6 but they did not compute the bifurcation diagrams.

Next, we will see how the bifurcation diagram changes as κ changes. Figure 7 shows the bifurcation diagram for $\kappa=2$ and the highest wave profiles of mode 1 and mode 2. Branches of mode 1 emanate downward but almost horizontally. Similarly to the case of $\kappa=0.7$, branches of mode 1 and of mode 2 are symmetric about μ-A_2 plane and μ-A_1 plane respectively. Profiles of the highest waves look like those of $\kappa=0.7$, but the enclosed bubbles and the wave amplitude are larger than them. We could not catch any secondary bifurcation. As κ becomes larger, the inclination of the branch of mode 1 becomes upward. And the simple bifurcation point of mode 1 and mode 2 separate further from each other. The enclosed bubbles and the wave amplitude of the highest waves become larger. We see such changes continuously from Figure 6 for $\kappa=0.7$ to Figure 8 for $\kappa=\infty$. These are major changes for $\kappa>0.7$.

On the other hand, qualitatively different changes appear for $\kappa<0.7$. The first is that there appears a turning point. The second is that the secondary bifurcation branches emanate from the upper side or the lower side of the branch of mode 2 when $\kappa>0.5$ or $\kappa<0.5$, respectively. The third is that the wave of mode 1 changes its profile whether κ is larger than $1/m$ $(m=1, 2, \cdots)$ or not. Figure 9 shows the case of $\kappa=0.55$. The secondary bifurcation branches also emanate from the upper side

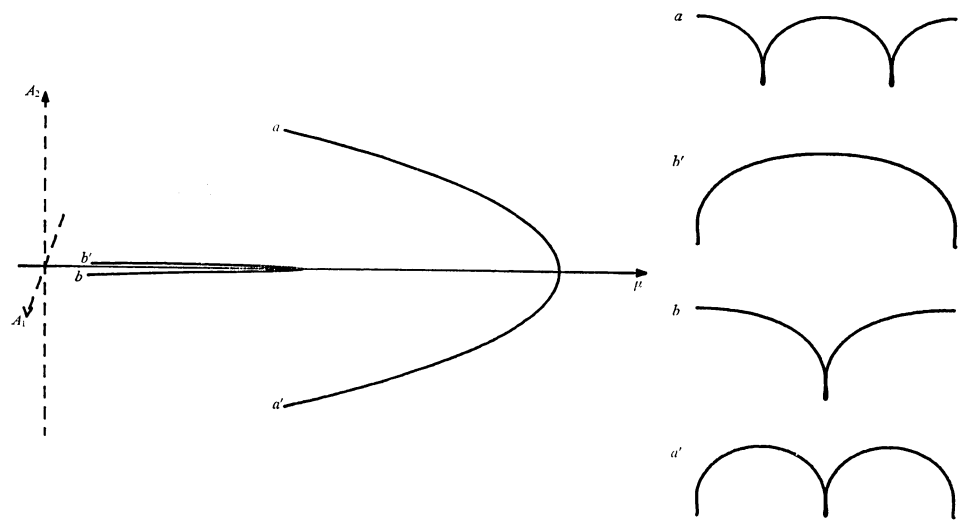

Figure 7. Bifurcation branches for $\kappa=2$ of infinite depth.

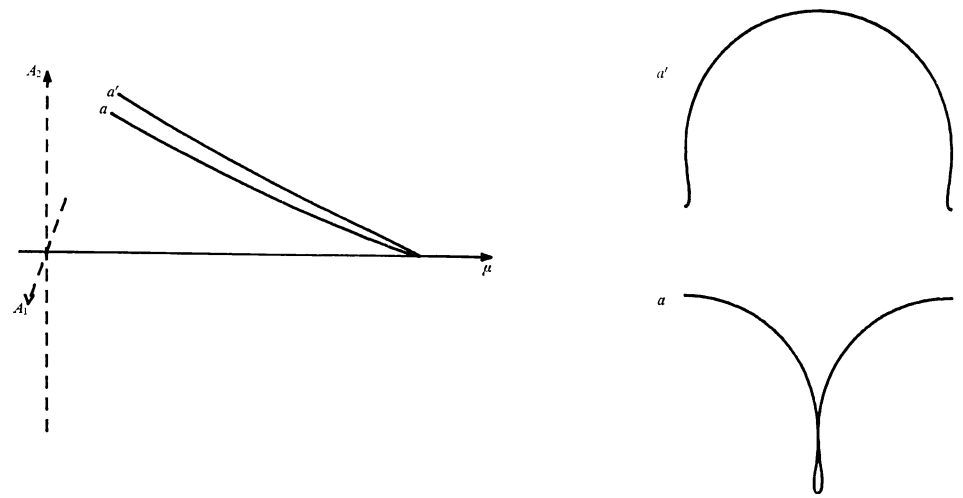

Figure 8. Bifurcation branches for $\kappa=\infty$ of infinite depth.

of the branch of mode 2. However, the bifurcation is supercritical and there appears a turning point on secondary branches.

Figure 10 shows the case of double bifurcation of mode (1, 2), i.e. $\kappa=0.5$. In the upper side of the branches of mode 1, there is a turning

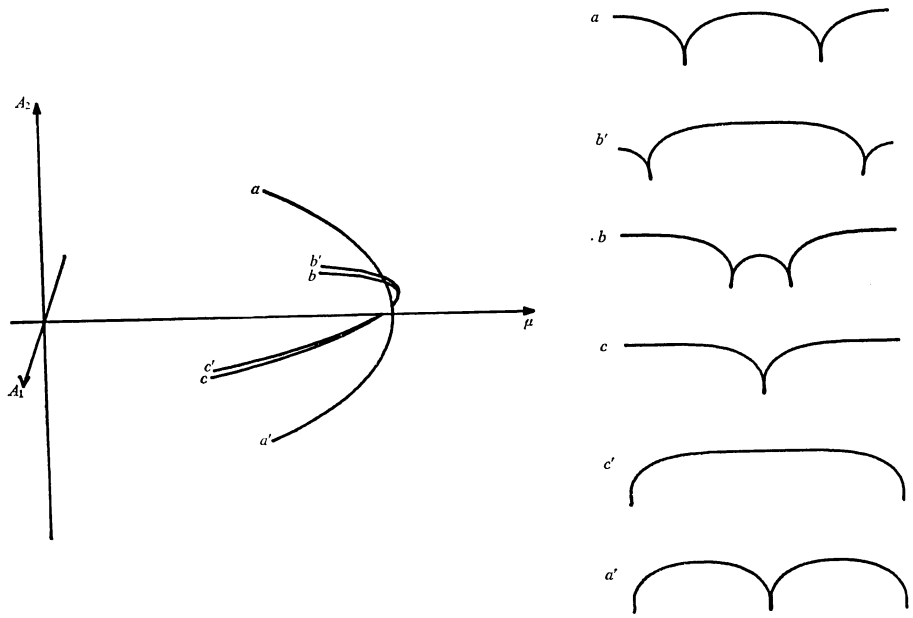

Figure 9. Bifurcation branches for $\kappa=0.55$ of infinite depth.

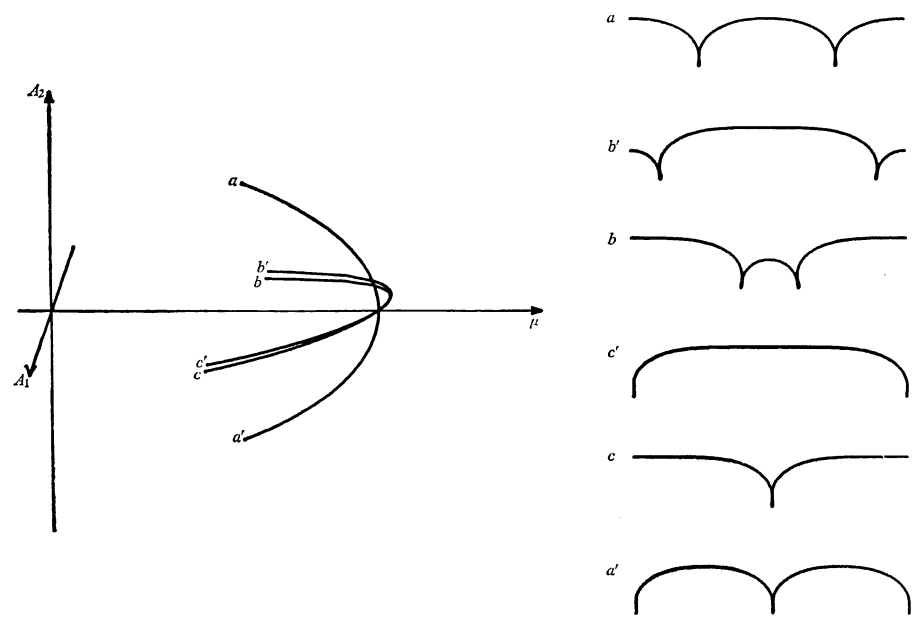

Figure 10. Bifurcation branches for $\kappa=0.5$ of infinite depth.

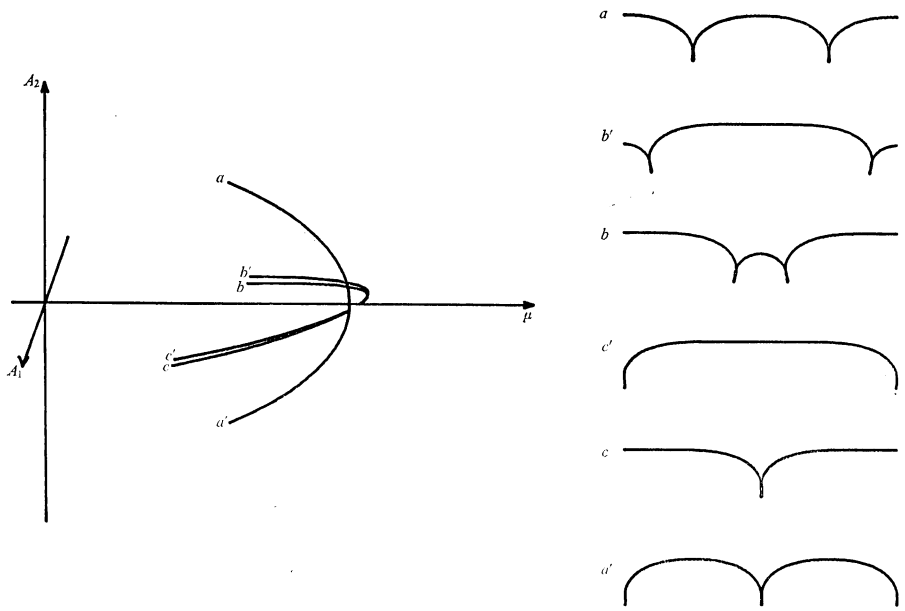

Figure 11. Bifurcation branches for $\kappa=0.45$ of infinite depth.

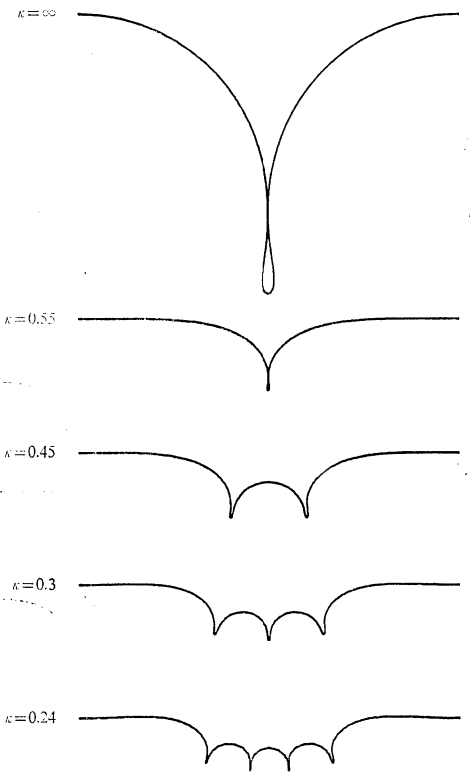

Figure 12. Profiles of waves which are bifurcations of mode 1.

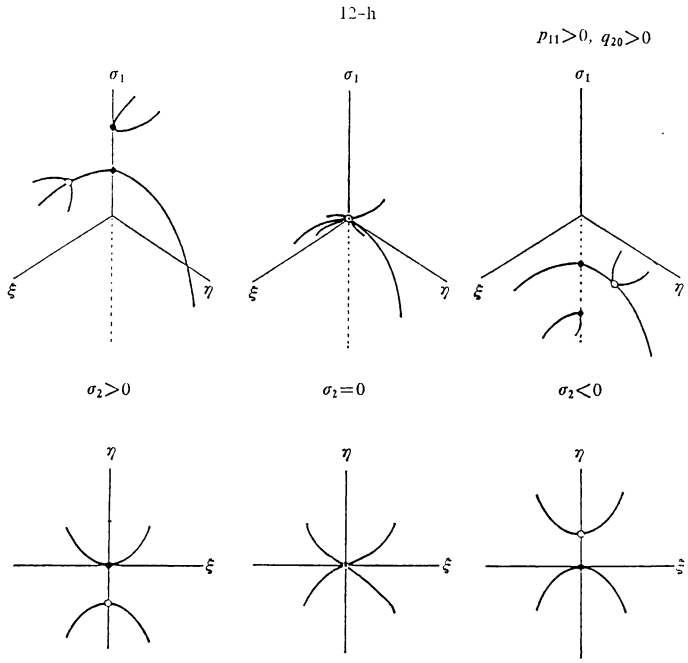

Figure 13

point. We remark the branches of mode 1 are transcritical. Figure 11 shows the case of $\kappa=0.45$. The secondary branches emanate from the lower side of the branch of mode 2. The branches of mode 1 have a turning point. When $\kappa<0.45$, the bifurcation diagram is similar to the one of $\kappa=0.45$. However, solutions of mode 1 change their profiles when the value of κ crosses $1/m$ $(m=1, 2, \cdots)$, which corresponds to the double bifurcation point of mode $(1, m)$. In Figure 12, we show the variation of wave profiles of the branch of mode 1 for various values of κ. For $\kappa \in (1/(m+1), 1/m]$, the waves of mode 1 have m dents. We remark that all the bifurcation points are pitchforks or limit points except for Figure 10.

We now study the above results by mathematical means. Details will be given in the following paper [15]. The basis of our theory is $O(2)$-equivariance of the equation. To use $O(2)$-equivariance, which we will state below, we need to take account of those waves whose Stokes coefficients B_j are not necessarily zero. Since we are now considering general $(A_1, \cdots, B_1, \cdots)$, (10) is replaced by the following

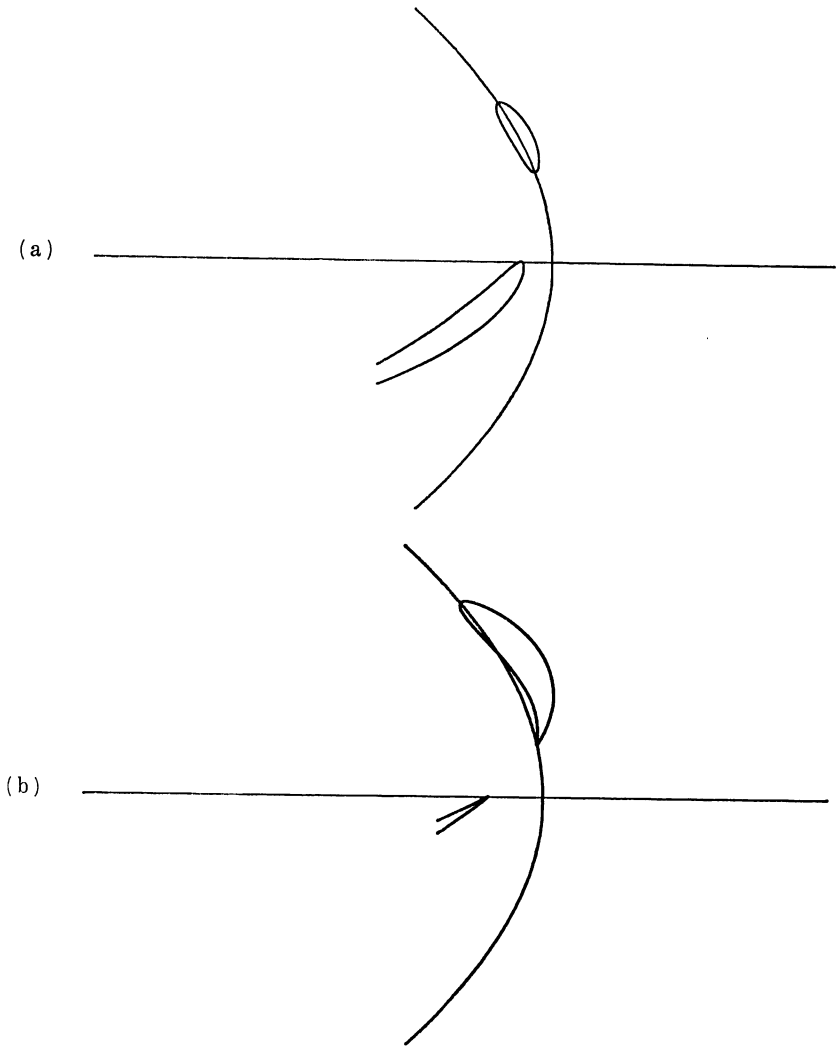

Figure 14

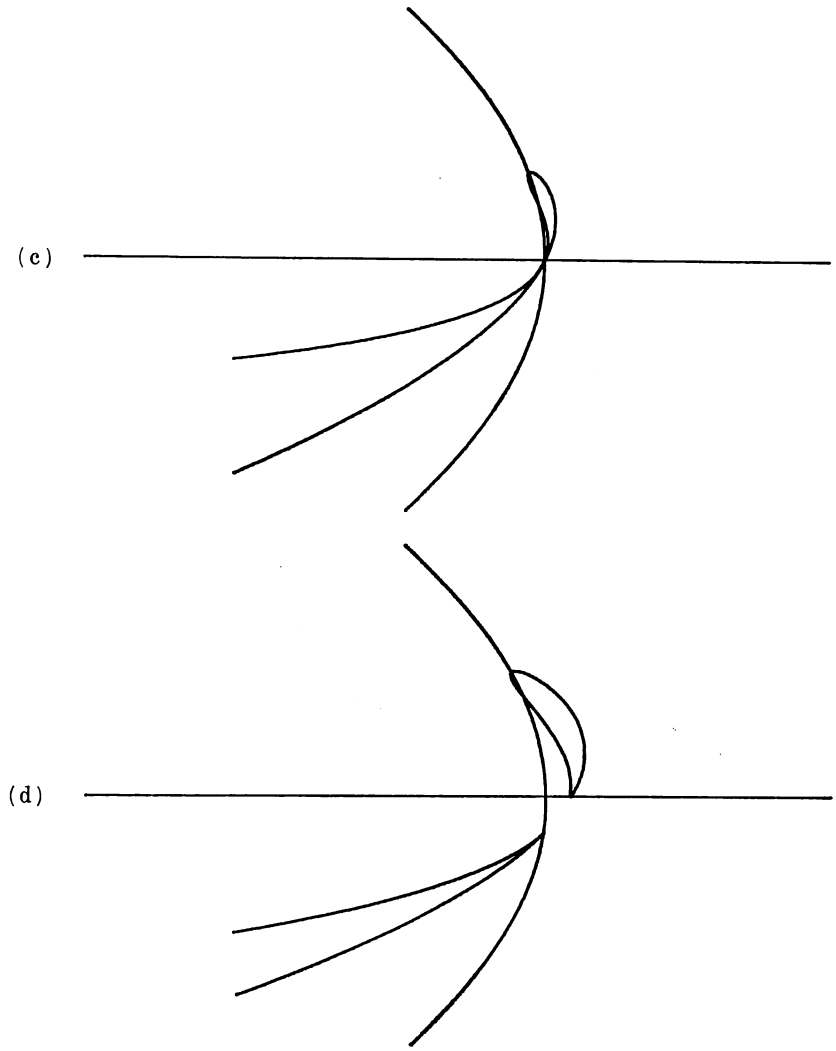

Figure 14

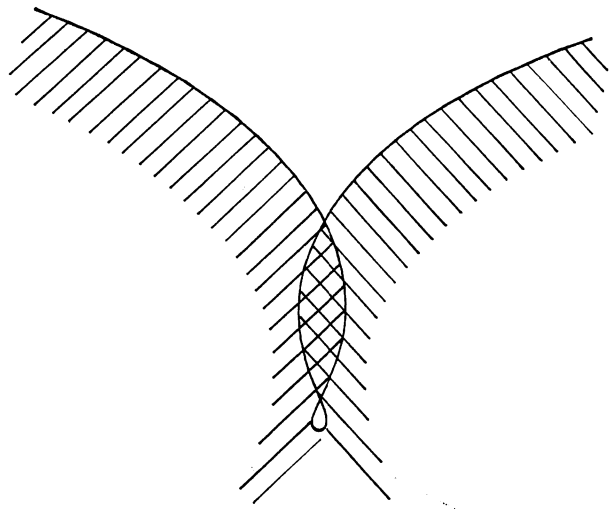

Figure 15. Profile of overlapped wave.

$$(23)\qquad \begin{cases} X'(\xi)=1+\sum_{1}^{\infty}\{A_j\cos(j\xi)+B_j\sin(j\xi)\}, \\ Y'(\xi)=\sum_{1}^{\infty}\{-A_j\sin(j\xi)+B_j\cos(j\xi)\}. \end{cases}$$

We note that (6) is a periodic function of $\mathrm{Re}(w)$. This fact enables us to define a natural action of $O(2)$ on $(A_1, A_2, \cdots, B_1, B_2, \cdots)$. To this end we define an action of $O(2)$ on w:

$$(24)\qquad \begin{cases} w \longrightarrow w+\dfrac{cL\alpha}{2\pi} \qquad (0\leq\alpha<2\pi), \\ w \longrightarrow \bar{w}. \end{cases}$$

Here $\alpha\in[0, 2\pi)$ corresponds to the rotation in $\boldsymbol{R}^2$ of angle α. The complex conjugacy corresponds to the reflection with respect to the x-axis. This action of $O(2)$ defines the following action on $(A_1, A_2, \cdots, B_1, B_2, \cdots)$

$$(25)\qquad \begin{cases} (A_n, B_n) \longrightarrow (A_n\cos(n\alpha)+B_n\sin(n\alpha),\ -A_n\sin(n\alpha)+B_n\cos(n\alpha)), \\ (A_n, B_n) \longrightarrow (A_n, -B_n). \end{cases}$$

The above relation comes from (24) if we put $V=0$ in (6) and substitute w with the right hand side of (24) (see also [15]). We now redefine F in (14). The modification is easy:

$$F(\kappa, \mu;\ A_1, A_2, \cdots, B_1, B_2, \cdots)=(A_1^*, A_2^*, \cdots, B_1^*, B_2^*, \cdots), \tag{26}$$

where A_j^* and B_j^* are defined by (11, 12, 13) with (10) replaced by (23). Then it is easy to check that F is $O(2)$-equivariant with respect to (25). By $O(2)$-equivariance, we mean that, if the replacement (25) occurs, then the right hand side is transformed according to

$$(A_n^*, B_n^*) \longrightarrow (A_n^* \cos(n\alpha)+B_n^* \sin(n\alpha),\ -A_n^* \sin(n\alpha)+B_n^* \cos(n\alpha)),$$
$$(A_n^*, B_n^*) \longrightarrow (A_n^*, -B_n^*).$$

This property enables us to simplify the bifurcation equation. The simplification is due to [5, 6]. Figure 13 is borrowed from [5] and is a picture of the bifurcation diagrams near the double bifurcation point of mode (1, 2) which is drawn from the simplified bifurcation equation. We notice that Figures 9, 10, 11 include Figure 13 as a subset. Ours are, however, more complicated than Figure 13.

The key idea to explain these complicated phenomena is, as in [6, 12], a degeneracy in the bifurcation equation. Figures 14a–14d are given in [12] by an abstract theory of degenerate bifurcations. Let us compare Figures 6, 9, 10 and 11 with Figures 14a, 14b, 14c and 14d, respectively. Then we observe that the formers are subsets of the latters. This difference does not imply inappropriateness of the theory. Instead, the difference suggests necessity of further computations. The reason is as follows: We computed Figures 6–11 by tracing the solutions until they lose physical meaning. Namely, at the end points in each branch, the wave profiles make contact points. This, however, does not imply the ends of the diagrams. The equation (14) contains those solutions which have self-intersections in the wave profiles (see Figure 15). Such solutions are physically meaningless. But they have equally rigorous meaning as solutions of (14). Therefore it will be worthwhile to continue computing further.

We will show the results and compare again with Figure 14a–d below. We would like to examine whether the branch of mode 1 or secondary branch would join with mode 2 branch as in Figure 14. Figures 16a and 16b are extended results of Figures 3–6 for $\kappa=0.7$. After the highest waves in Figures 3–5, they become self-intersecting waves and the fluid regions are overlapped as shown in Figure 15. Namely they are meaningless waves in a physical sense. Figures 16a–b show the change of the wave profiles as we trace the secondary branch until we

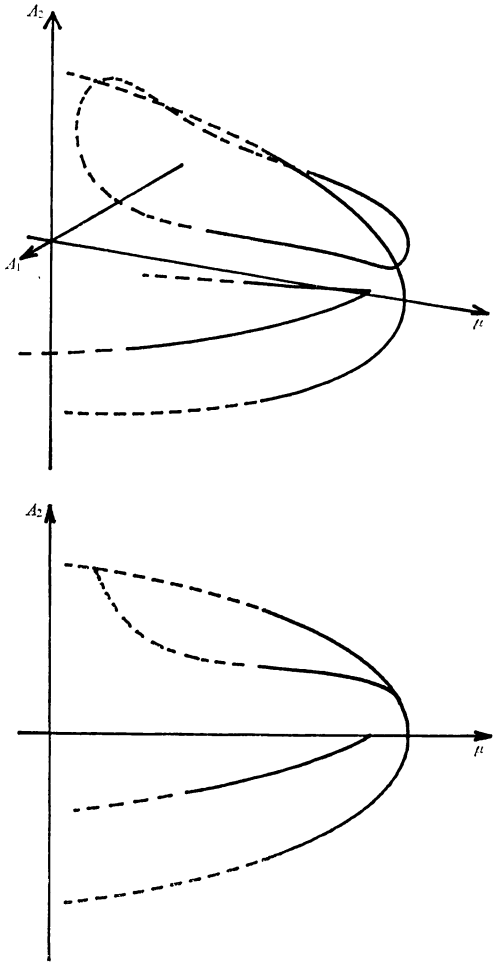

Figure 16a. Bifurcation diagram of mode 1 and 2 for $\kappa=0.7$.

come back to wave of mode 2. All the lowest parts of self-intersecting waves appear to have sharp corners, but they are actually smooth curves as in the magnified figure within the dotted circle. In the bifurcation diagram of Figure 16a, dotted curves indicate solutions which have self-intersections. Figures 17-19 for $\kappa \geq 0.5$ also show that waves bifurcating from the branch of mode 2 certainly connect with the branch of mode 2 again. Consequently Figures 16 and 17 are qualitatively the same as Figure 14a, where there is no turning points. Figure 18 agrees qualita-

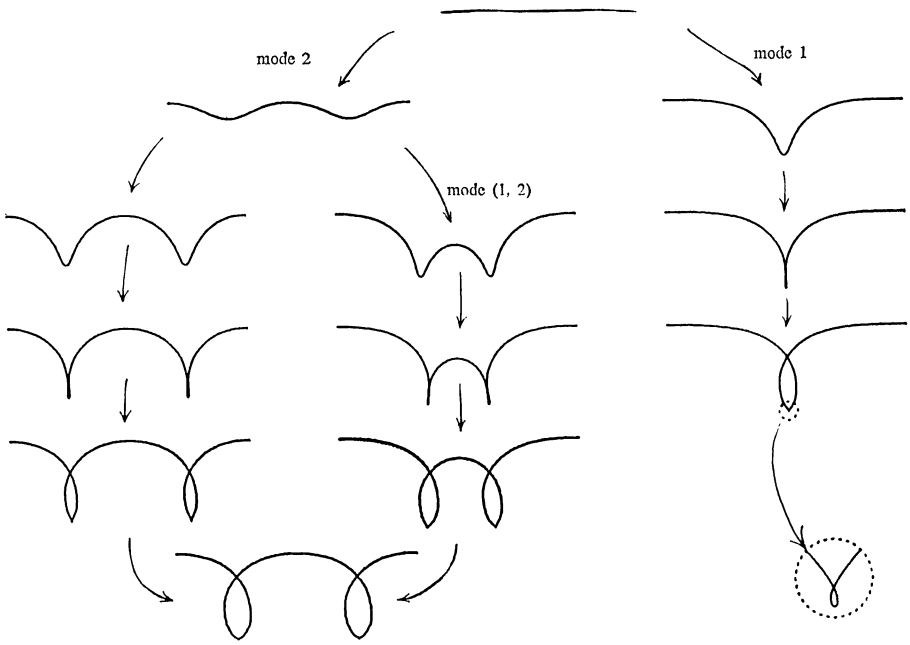

Figure 16b. Profiles of bifurcation waves for $\kappa=0.7$ of infinite depth.

tively with Figure 14b, where there are turning points. Figure 19 agrees qualitatively with Figure 14c, which is the case of double bifurcation point. The branch of mode 1 in Figure 20 is unfinished and the computation is not sufficient so as to identify Figure 20 as Figure 14d. However, by considering that joining point to the branch of mode 2 approaches to A_2-axis as κ decreases, it can be imagined that Figure 20 may have a joining point in $\mu<0$. In fact we caught no singular points on the branch of mode 2 in $\mu>0$. Then we can regard that Figure 20 agrees qualitatively with Figure 14d, although a computational difficulty prevent us from checking the existence of the joint.

Thus far, we have restricted our attention to the case of infinite depth. We now consider the influence of the depth of the flow. We assume that the bottom is the x-axis: $\{y=0\}$. Accordingly, the flow region is $\{(x, y);\ |x|<L/2,\ 0<y<H(x)\}$. We seek a complex potential $U+iV$ satisfying

$$U\left(\pm\frac{L}{2}, y\right)=\pm\frac{cL}{2} \qquad \text{(respectively)},$$

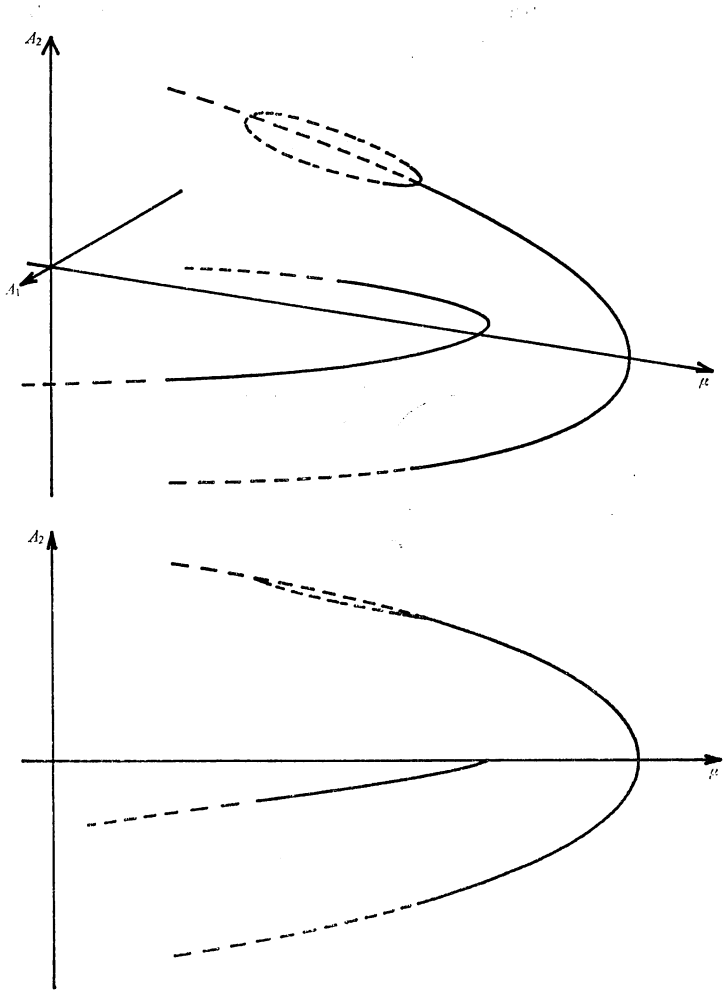

Figure 17. Bifurcation diagram of mode 1 and 2 for $\kappa=1.3$.

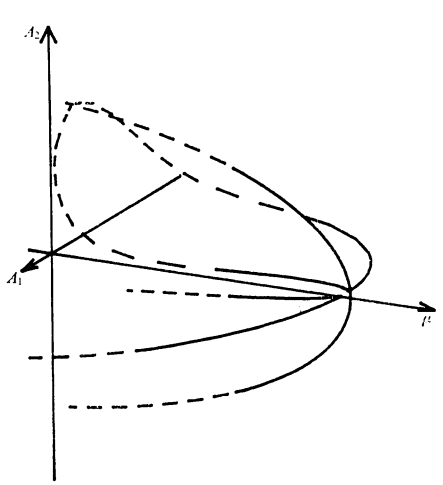

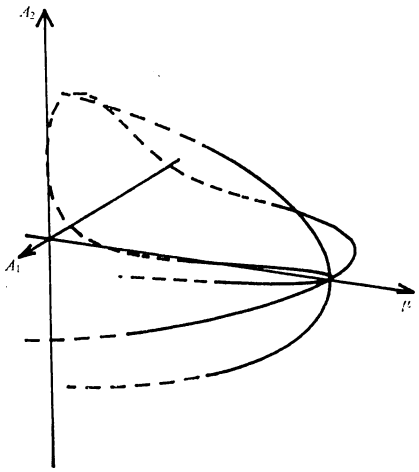

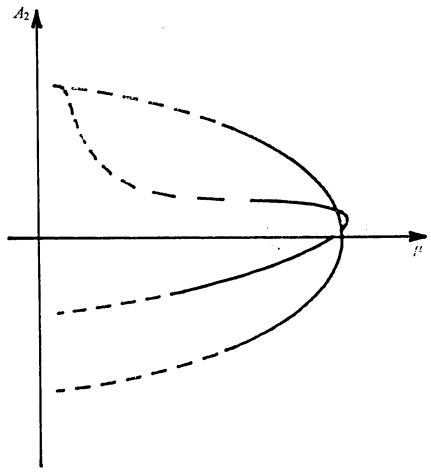

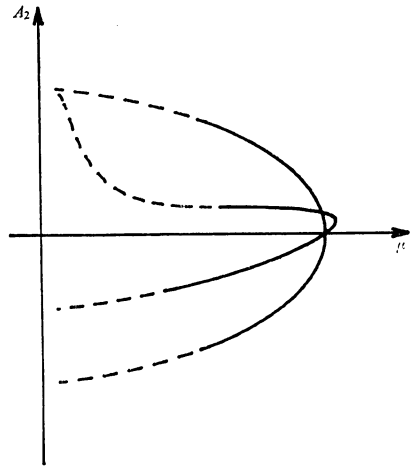

Figure 18 Figure 19

Figure 18. Bifurcation diagram of mode 1 and 2 for $\kappa=0.55$.
Figure 19. Bifurcation diagram of mode 1 and 2 for $\kappa=0.5$.

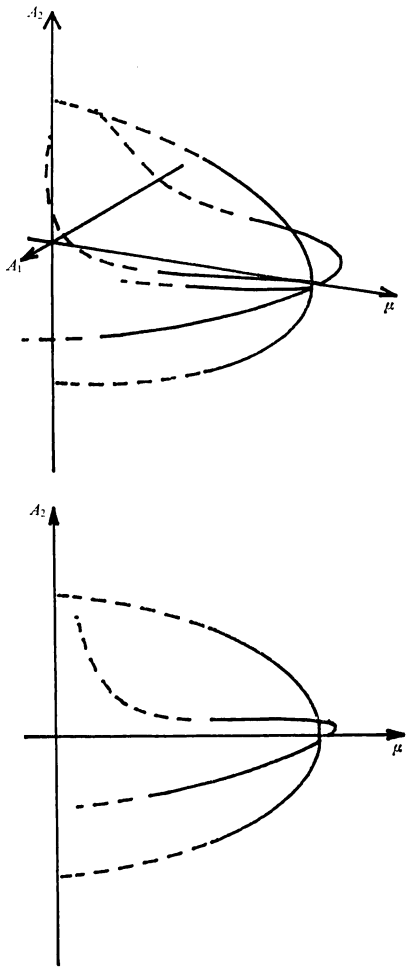

Figure 20. Bifurcation diagram of mode 1 and 2 for $\kappa=0.45$.

$$V=\text{constant} \qquad \text{on} \quad y=H(x) \quad \text{and} \quad y=0,$$

$$\frac{1}{2}\left|\frac{dw}{dz}\right|^2+gy-TK=\text{constant} \qquad \text{on} \quad y=H(x).$$

We may normalize $V\equiv 0$ on $y=H(x)$. We put $V=-a$ on $y=0$. The constant a depends on the depth and the propagation speed c. Note that a is larger if the flow is deeper. The Stokes expansion (6) should be modified so that $w=U+iV=U-ia$ corresponds to $z=x\in R$. We put

$$\begin{aligned}(27)\qquad z&=x+iy\\ &=\frac{w}{c}+\sum_{j=1}^{\infty}\frac{iL}{2\pi j}\left[A_j\sinh\left(-\frac{2j\pi(iw-a)}{cL}\right)\operatorname{cosech}\left(\frac{2j\pi a}{cL}\right)\right.\\ &\quad\left.+iB_j\cosh\left(-\frac{2j\pi(iw-a)}{cL}\right)\operatorname{sech}\left(\frac{2j\pi a}{cL}\right)\right]+\frac{iL(A_0+iB_0)}{2\pi}.\end{aligned}$$

By this ansatz we have the following parametrization of the free boundary

$$\begin{cases} x=\dfrac{U}{c}+\dfrac{L}{2\pi}\displaystyle\sum_1^{\infty}\frac{A_j}{j}\coth\left(\frac{2j\pi a}{cL}\right)\sin\left(\frac{2j\pi U}{cL}\right)+\frac{LB_0}{2\pi},\\ y=\dfrac{L}{2\pi}\displaystyle\sum_1^{\infty}\frac{A_j}{j}\cos\left(\frac{2j\pi U}{cL}\right)+\frac{LA_0}{2\pi}.\end{cases}$$

By the same nondimensionalization as before, we have

$$(28)\qquad X(\xi)=\xi+\sum_1^{\infty}\frac{A_j}{j}\coth(j\nu)\sin(j\xi)+B_0, \qquad Y(\xi)=\sum_1^{\infty}\frac{A_j}{j}\cos(j\xi)+A_0,$$

where $\nu=2\pi a/(cL)$. The problem is to solve (8′) with the parametrization (28). Note that a new parameter $\nu\in(0,\infty)$ is now introduced. If we allow ν to be infinity, then (28) reduces to (7). Consequently, the flow of infinite depth is included in the new problem. We also note that the definition of F in (14) should be modified, too. A_j^* in (12) remains unchanged. But B_j^* should be defined by

$$B_j^*=-\frac{1}{\pi}\coth(j\nu)\left(\frac{d}{d\xi}\Psi(\xi),\cos(j\xi)\right)=-\frac{1}{\pi}\coth(j\nu)(\Psi(\xi),j\sin(j\xi)).$$

By this modification, we see that F is commutative with the action of $O(2)$, which is defined by

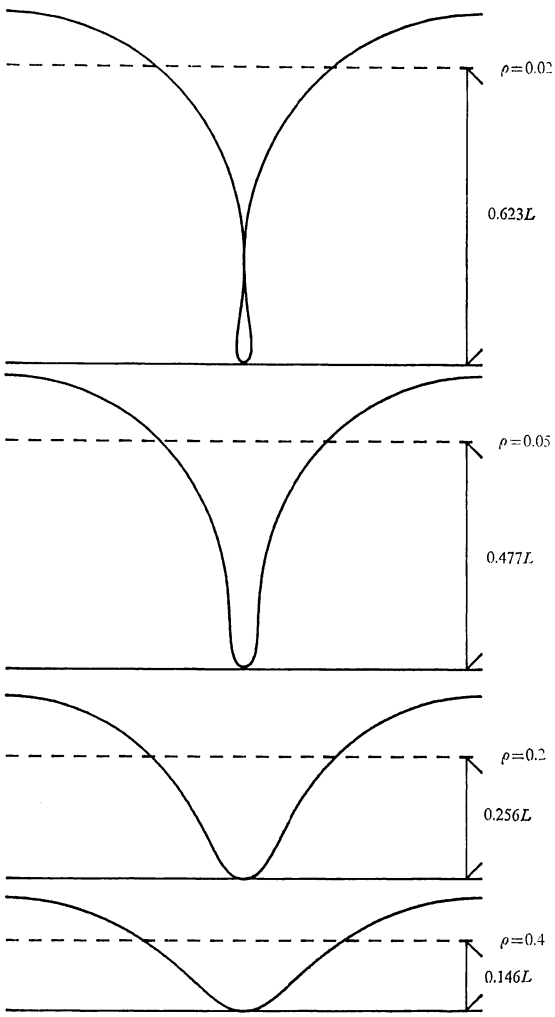

Figure 21. Profiles of waves of almost maximum height for different depths.

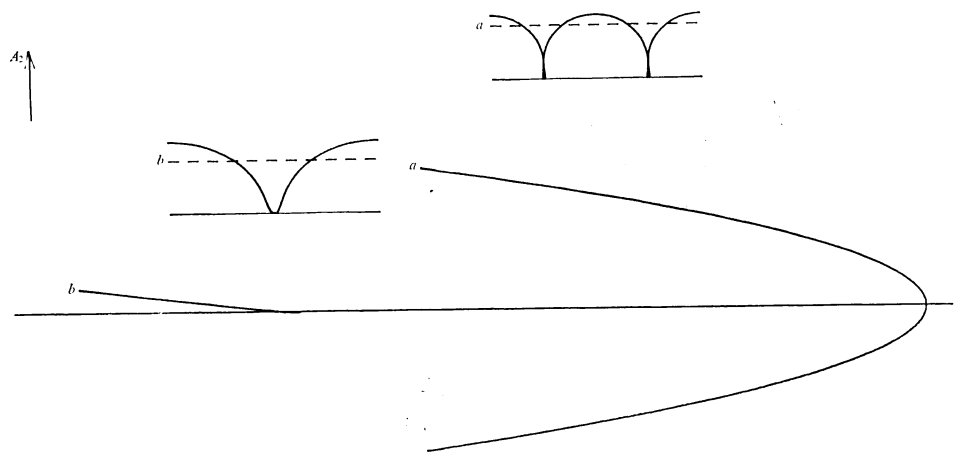

Figure 22. Bifurcation branches and profiles of solutions for $\kappa=4.0$ and $\rho=0.2$.

$$\begin{cases} (A_n, B_n) \longrightarrow (A_n \cos(n\alpha)+B_n \tanh(n\nu)\sin(n\alpha), \\ \qquad\qquad -A_n \coth(n\nu)\sin(n\alpha)+B_n \cos(n\alpha)), \\ (A_n, B_n) \longrightarrow (A_n, -B_n). \end{cases}$$

We will see how bifurcation structures change as the depth of fluid becomes shallower. Now we introduce a parameter $\rho=\exp(-2\nu)$. $\{1>\rho\geq 0\}$ corresponds to $\{0<\nu\leq\infty\}$.

In Figure 21 we show profiles of pure capillary waves (namely the case of $\kappa=\infty$) in four values of depth, $\rho=0.02$, 0.05, 0.2 and 0.4. These values of ρ correspond to the depth of $0.623L$, $0.477L$, $0.256L$ and $0.146L$, respectively. For $\rho\leq 0.02$, profiles of pure capillary waves are similar to Kinnersley's waves. For $\rho>0.02$, a depressed part of the wave touches the bottom of fluid before the wave encloses a bubble.

Now we put $\rho=0.2$, then the depth of fluid is $0.256L$. Figures 22–26 show bifurcating solutions and diagrams near the double bifurcation point of mode (1, 2). Dotted curves in diagrams indicate solutions with self-intersections as before. Dotted lines in wave profiles indicate mean water level. Figure 22 shows the case of $\kappa=4.0$. There is no secondary bifurcations. The highest wave of mode 2 encloses two bubbles and just touches the bottom of fluid. The highest wave of mode 1 does not reach to enclose a bubble. Figure 23 shows the case of $\kappa=0.55$. There are two secondary bifurcations which emanate subcritically from the upper part of the branch of mode 2 with no turning point and connects again with the branch of mode 2. Figure 24 shows the case of $\kappa=0.45$.

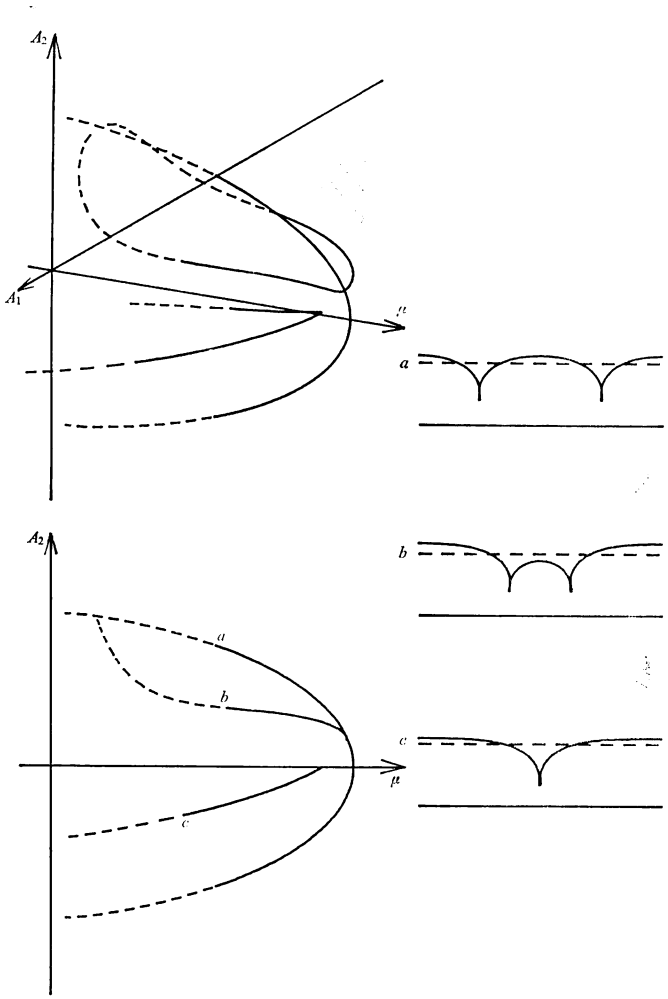

Figure 23. Bifurcation branches and profiles of solutions for $\kappa=0.55$ and $\rho=0.2$.

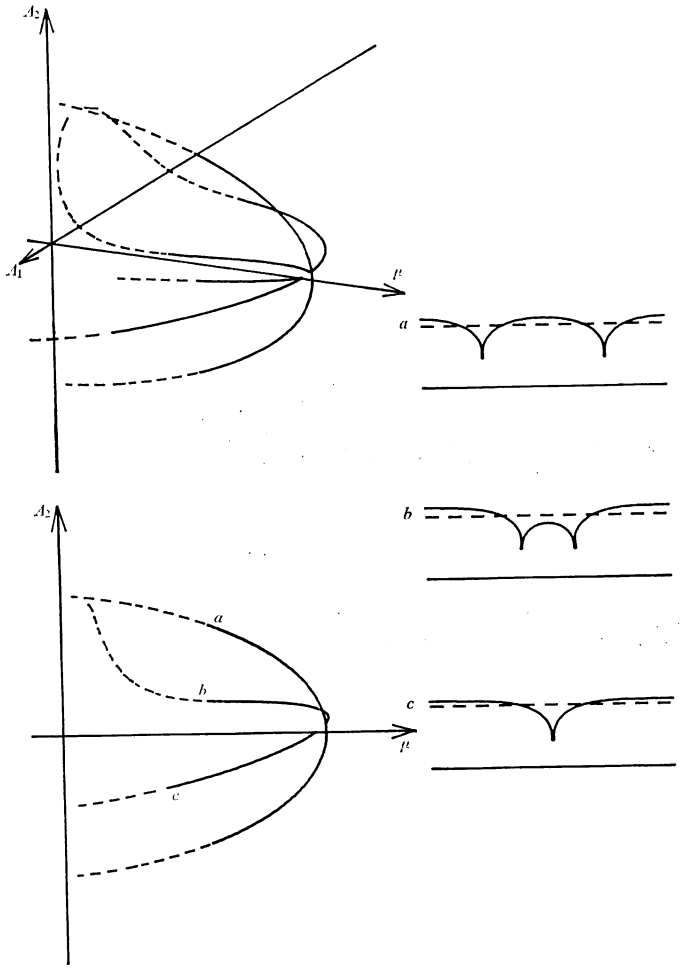

Figure 24. Bifurcation branches and profiles of solutions for $\kappa=0.45$ and $\rho=0.2$.

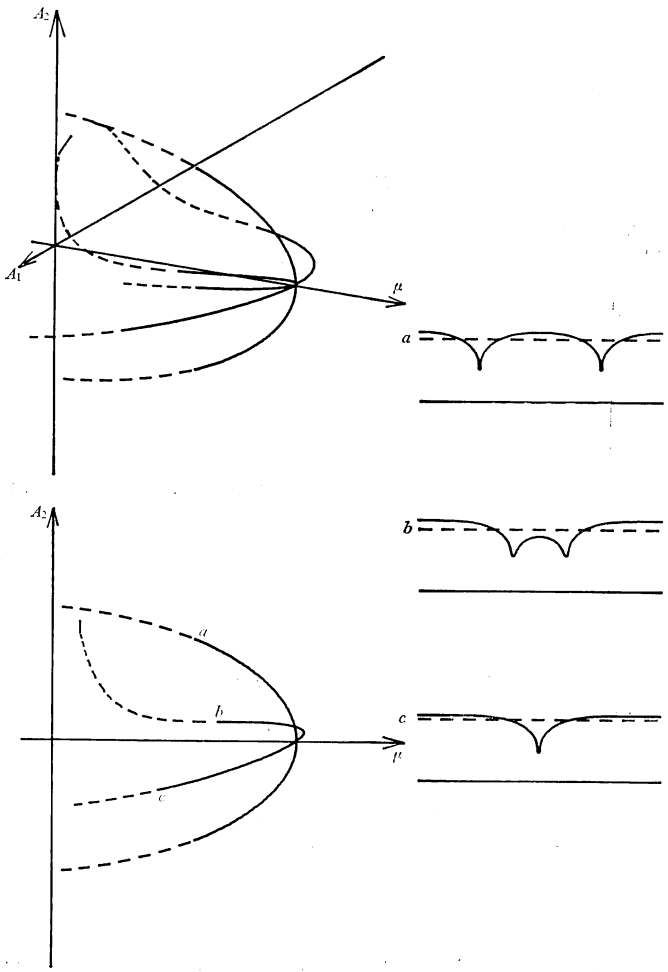

Figure 25. Bifurcation branches and profiles of solutions for $\kappa=0.4$ and $\rho=0.2$.

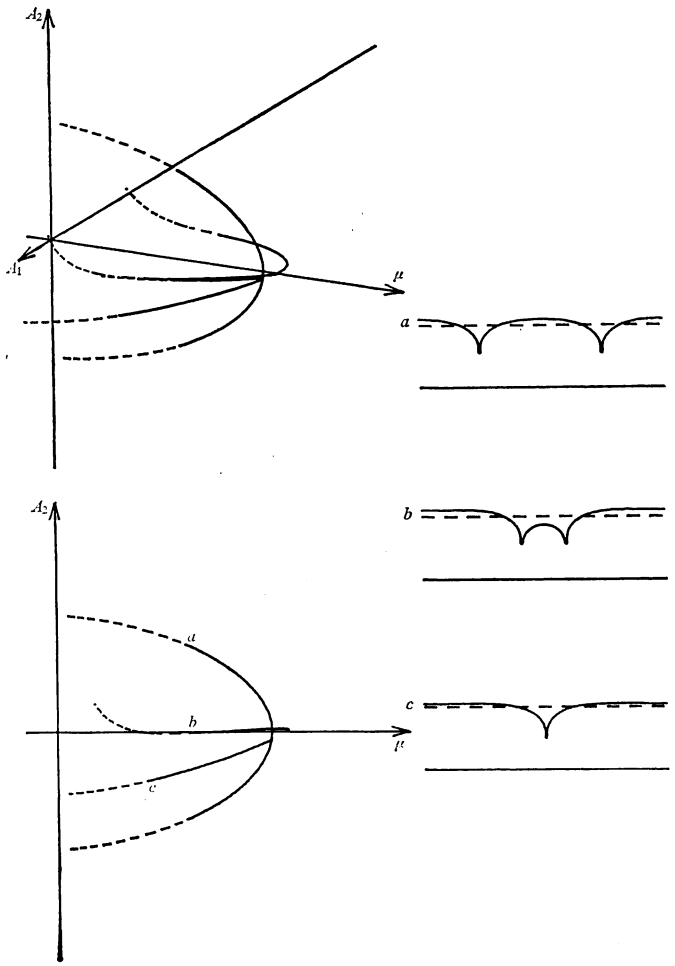

Figure 26. Bifurcation branches and profiles of solutions for $\kappa=0.32$ and $\rho=0.2$.

Each of the secondary branches has a turning point and it connects again with the branch of mode 2. Figure 25 shows the case of double bifurcation point of mode (1, 2) and $\kappa=0.4$. We could not extend the computation until the branch of mode 1 meet that of mode 2 again. In Figure 26, the case of $\kappa=0.32$ is shown. Secondary bifurcations emanate from the lower part of mode 2 branch. The branches of mode 1 has a turning point.

As we have seen, Figure 21-26 are similar to the results of infinite depth. As far as we can compute, we could not find any significant change in bifurcation structures by a change of the depth. All the free surface of the highest waves in Figure 23-26 do not touch the bottom of fluid. The reason why tracing of branches become hard does not come from physical meaning. Rather, the difficulty lies in the fact that the matrix condition becomes worse in the Euler-Newton iteration.

§ 3. Results for the bifurcation of mode (1, 3).

In this section we show the results on the interaction of mode 1 and mode 3. We only show the results of infinite depth, since we could not find any significant difference between those of finite depth and of infinite depth.

We consider the case of $m=1$ and $n=3$. Let (κ_0, μ_0) be the double bifurcation point of mode (1, 3). Then from (15), we have $\kappa_0=1/3$ and $\mu_0=4/3$. By a perturbation of κ from κ_0, we see variety of bifurcation structures near the double bifurcation point of mode (1, 3). Each of Figures 27-32 consists of three diagrams (i), (ii), (iii) and wave profiles (iv). Figures (i$\sim$iii) are viewed from three different directions. (ii) is a view from μ-axis. (iii) is a view from A_3-axis. We give profiles of bifurcating solutions in (iv). Meaning of dotted part of bifurcation branch is the same as in § 2. Figure 27 shows the case of $\kappa=0.3<\kappa_0$. The branches of mode 1 and mode 3 are bifurcating from trivial solution. Difference from the bifurcation of mode (1, 2) is that there exist another branches located apart from them. Figure 28 is concerned with the case of the double bifurcation point of mode (1, 3), from which four different bifurcation branches are emanating. Figure 29 shows the case of $\kappa=0.35>\kappa_0$. Two secondary branches bifurcate from the branch of mode 3 transcritically. These two branches are symmetric about μ-axis. Figures 30-32 show the results for larger κ. When $\kappa=0.55$, each secondary branch crossing the branch of mode 3 extends to connect with the branch of

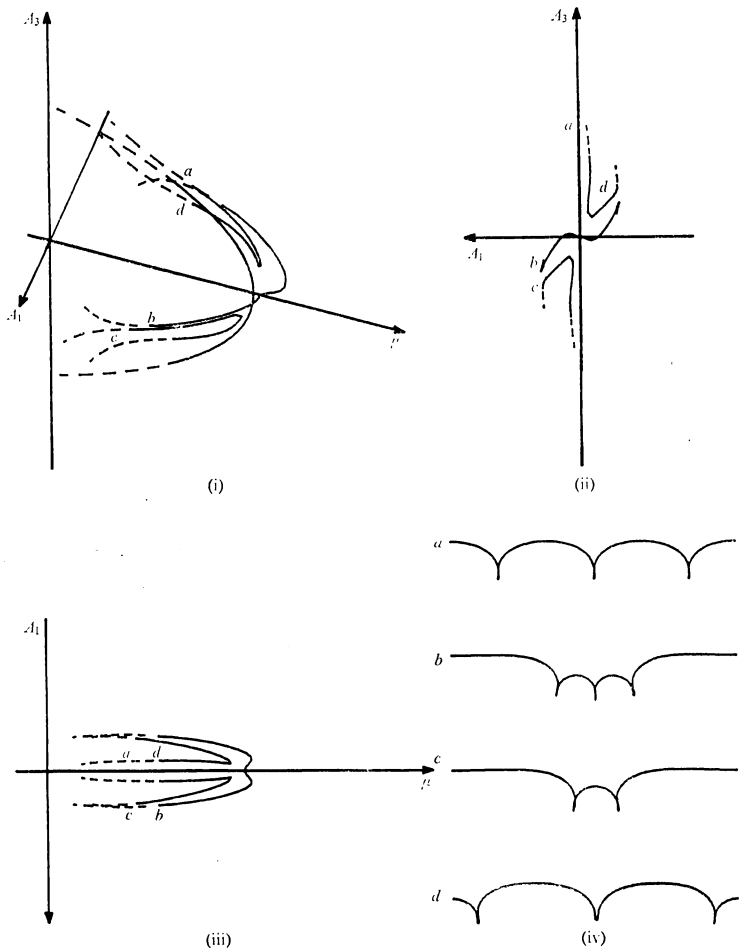

Figure 27. Bifurcation diagram of mode 1 and 3 for $\kappa=0.3$ of infinite depth.

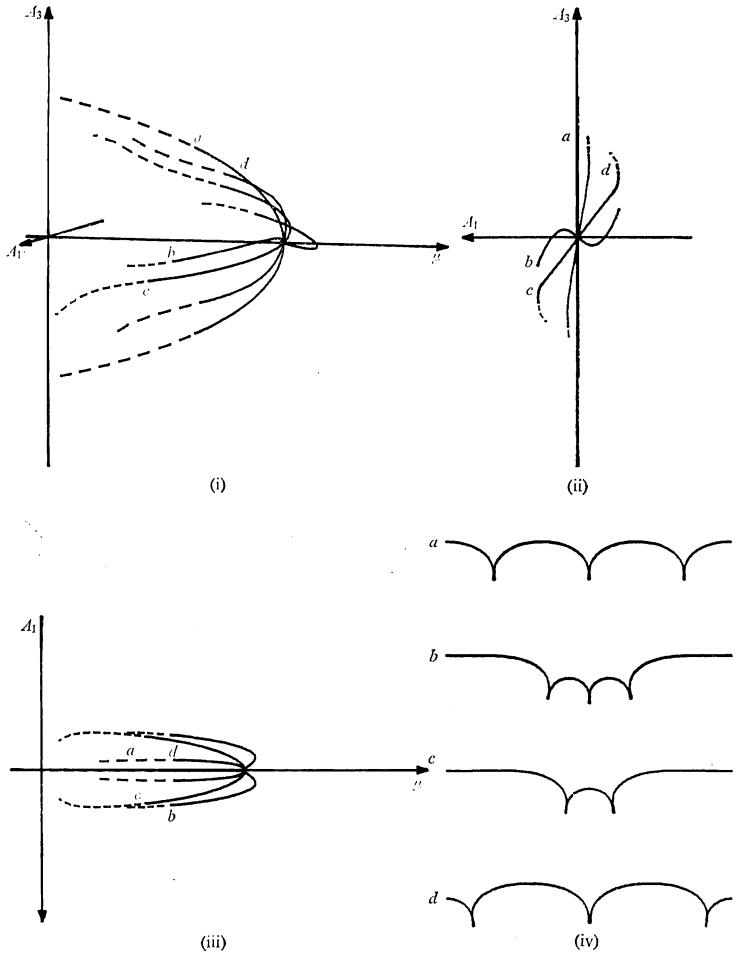

Figure 28. Bifurcation diagram of mode 1 and 3 for $\kappa=0.33$ of infinite depth.

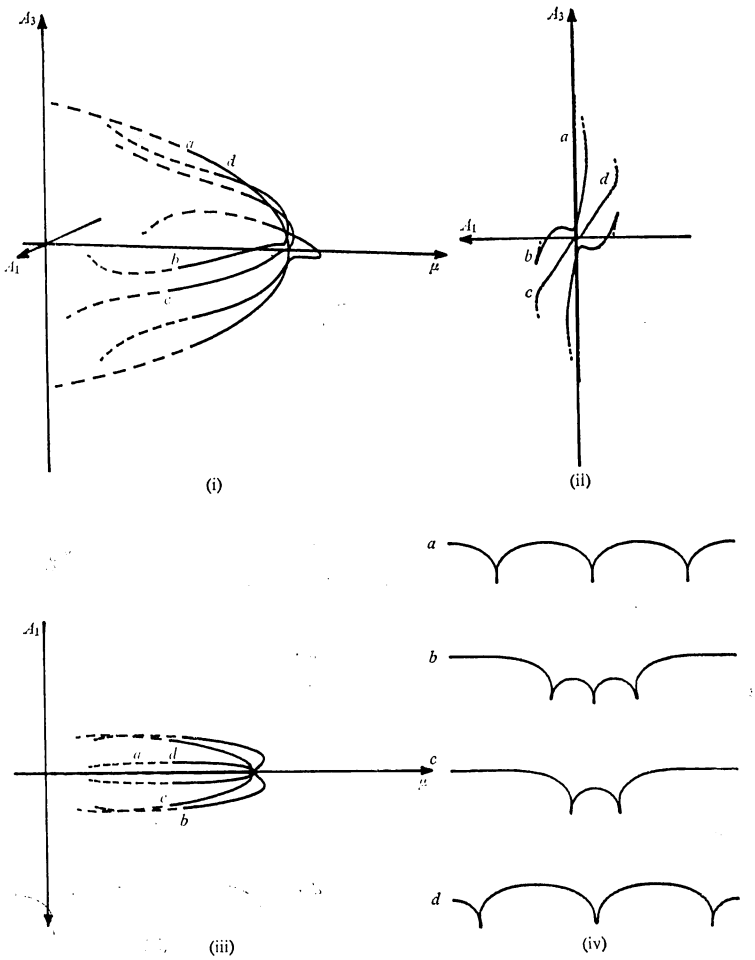

Figure 29. Bifurcation diagram of mode 1 and 3 for $\kappa=0.35$ of infinite depth.

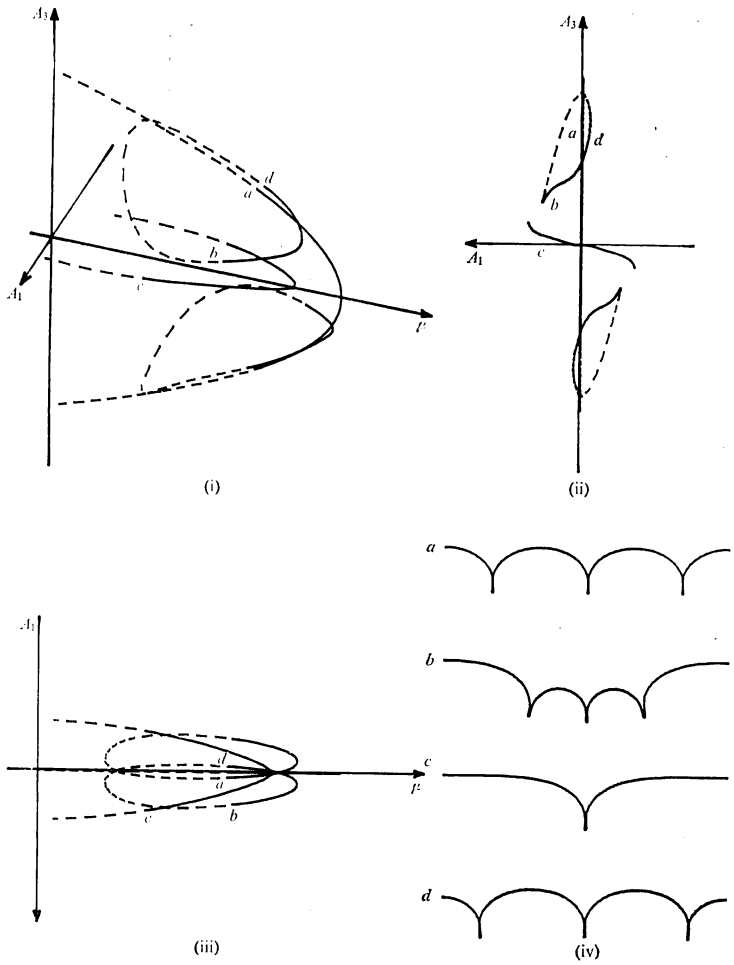

Figure 30. Bifurcation diagram of mode 1 and 3 for $\kappa=0.55$ of infinite depth.

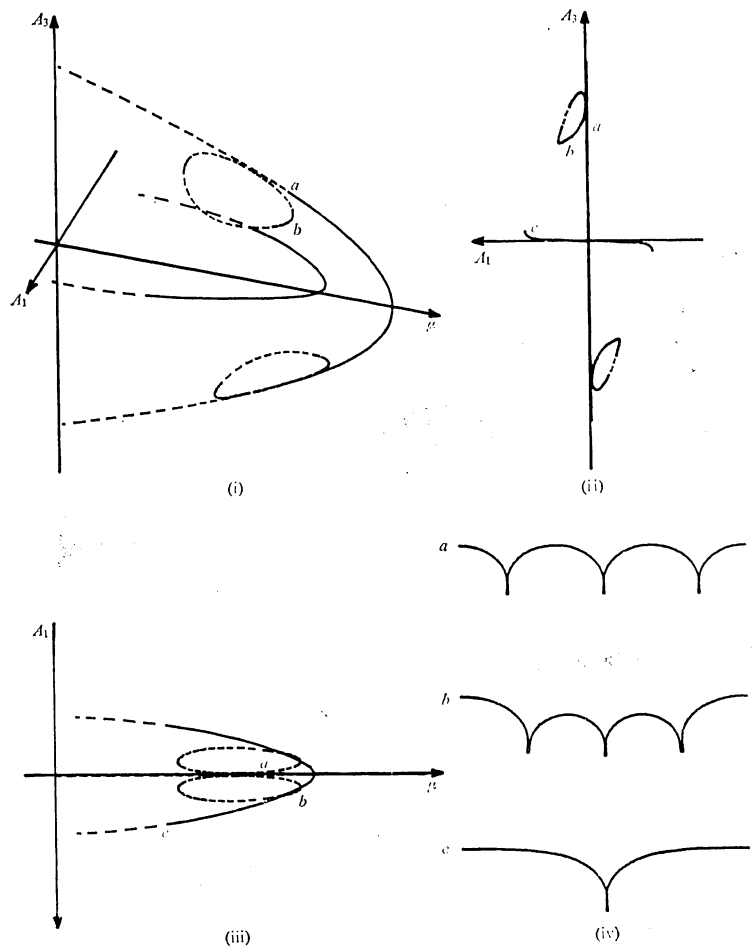

Figure 31. Bifurcation diagram of mode 1 and 3 for $\kappa=0.7$ of infinite depth.

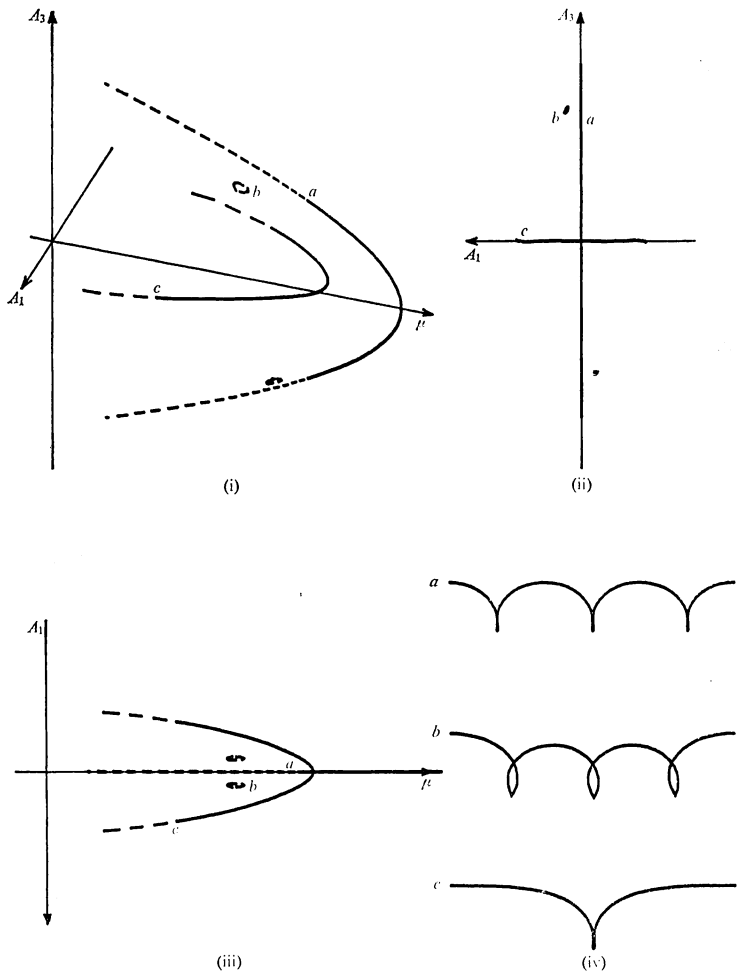

Figure 32. Bifurcation diagram of mode 1 and 3 for $\kappa=0.76$ of infinite depth.

mode 3 again as we can see in Figure 30. Namely the secondary branches form closed loops. As κ increases, emanating point and rejoining point on the branch of mode 3 approach each other. When $\kappa=0.7$, secondary bifurcation point disappears and the closed loops do not have intersections with the branch of mode 3 as shown in Figure 31. They are symmetric about μ-axis. As we increase κ, such closed loops become smaller and disappear (see Figure 32). These diagrams of Figures 30–32 are new bifurcation structures we have discovered.

§ 4. Conclusions.

We use the Stokes expansion method due to Chen and Saffman ([1, 2]). However, to make the bifurcation structures clear, we improved their procedure in the following sense: The first is that bifurcation theory given by [3, 9] is applied by using equation (8′) instead of (8), and then bifurcation diagrams are obtained. We showed that qualitative agreement of the numerical results with the mathematical analysis is guaranteed by considering not only ordinary solutions but also those which have self-intersections. The structures of our results for mode (1, 2) are new examples for $O(2)$-equivariant systems in that a turning point appears or disappears as one of bifurcation parameters changes. Such structures have analyzed only theoretically in [12].

For the results of mode (1, 3), the phenomena such as shown in Figures 30–32 seem to be new. Although we do not present a mathematical proof for the case of mode (1, 3), we discuss it in a forthcoming paper [15].

As a final remark, we mention some issues which are not treated in this paper. Although some other methods are applicable, the Stokes expansion method is useful and simple in the case of $\kappa\geq 0.24$ for infinite depth by the reasons that numerical integrations are not necessary by virtue of FFT method and that the Fréchet derivatives can be written explicitly. However, many interesting phenomena for small κ, especially asymptotic behavior to the pure gravity waves, can hardly be obtained by this method. Hogan ([7]) investigates such case by using the Padé approximation. His result, however, seems not to cover all the phenomena. There appears no qualitative differences between cases of finite and infinite depth as far as we can simulate. It may be possible that interesting phenomena will occur in cases of shallower depth. We hope to analyze such cases elsewhere.

Finally we note that Euler-Newton's iterations converge in 2~4 steps. We mainly compute by NEC PC-9801 and TOSBAC UX-700. We give an example of CPU time: it needs about 1 day to obtain whole branch of pure mode 2 for $\kappa=0.7$ and $\nu=\infty$ on NEC PC-9801 with a numeric processor.

References

[1] Chen, B. and P. G. Saffman, Steady gravity-capillary waves on deep water—I. Weakly nonlinear waves, Stud. Appl. Math. **60** (1979), 183-210.

[2] Chen, B. and P. G. Saffman, Steady gravity-capillary waves on deep water—II. Numerical results for finite amplitude, Stud. Appl. Math. **62** (1980), 95-111.

[3] Crandall, M. G. and P. H. Rabinowitz, Bifurcation from simple eigenvalue, J. Funct. Anal. **8** (1971), 230-263.

[4] Crapper, G. D., An exact solution for progressive capillary waves of arbitrary amplitude, J. Fluid Mech. **2** (1957), 532-540.

[5] Fujii, H., Mimura, M. and Y. Nishiura, A picture of the global bifurcation diagram in ecological interacting and diffusing systems, Phys. D **5** (1982), 1-42.

[6] Fujii, H., Nishiura, Y. and Y. Hosono, On the structure of multiple existence of stable stationary solutions in systems of reaction-diffusion equations, Stud. Math. Appl. vol. 18, North-Holland, Amsterdam, 1986, 157-219.

[7] Hogan, S. J., Some effects of surface tension on deep water waves, J. Fluid Mech. **91** (1979), 167-180; part 2, **96** (1980), 417-445; part 3, **110** (1982), 381-410.

[8] Kinnersley, W., Exact large amplitude capillary waves on sheets of fluid, J. Fluid Mech. **77** (1976), 229-241.

[9] Keller, H. B., Numerical solution of bifurcation and nonlinear eigen value problems, Applications of Bifurcation Theory, Academic Press, New York, 1977, 359-384.

[10] Levi-Civita, T., Détermination rigouresise des ondes permanents d'ampleur finie, Math. Ann. **93** (1925), 264-314.

[11] Nekrasov, A. I., On waves of permanent type I, Izo. Ivanovo-Voznesensk. Polit. Inst. **3** (1921), 52-65.

[12] Okamoto, H. and S. Tavener, A degenerate $O(2)$-equivariant bifurcation diagram and its application to the Taylor problem, preprint.

[13] Okamoto, H., $O(2)$-equivariant Bifurcation equations with two modes interaction, IMA preprint series #362, Inst. Math. and Appl., Univ. of Minnesota, Minnesota, 1987.

[14] Okamoto, H., On the problem of water waves of permanent configuration, Nonlinear Anal., to appear.

[15] Okamoto, H. and M. Shōji, in preparation.

[16] Reeder, J. and M. Shinbrot, On Wilton ripples, Arch. Rational Mech. Anal. **77** (1981), 321-347.

[17] Shōji, M., Thesis, University of Tokyo, Tokyo, 1989.

[18] Stokes, G. G., On the theory of oscillatory waves, Trans. Cambridge Phil. Soc. **8** (1847), 441-455.

[19] Struik, D. J., Détermination rigoureuse de ondes irrotationelles pèriodiques dans un canal á profondeur finie, Math. Ann. **95** (1926), 595-634.

[20] Toland, J. F. and M. C. W. Jones, The bifurcation and secondary bifurcation of

capillary-gravity waves, Proc. Roy. Soc. London Ser. A **399** (1985), 391-417.

(Received April 11, 1989)

Department of Mathematics
Faculty of Science
University of Tokyo
Hongo, Tokyo
113 Japan